catalysts

MDPI

Article

CO_2-Assisted Oxidative Dehydrogenation of Propane to Propylene over Modified SiO_2 Based Catalysts

Alexandra Florou [1], Aliki Kokka [1,*], Georgios Bampos [2] and Paraskevi Panagiotopoulou [1,*]

[1] Laboratory of Environmental Catalysis, School of Chemical and Environmental Engineering, Technical University of Crete, GR-73100 Chania, Greece; aflorou@tuc.gr
[2] Department of Chemical Engineering, University of Patras, GR-26504 Patras, Greece; geoba@chemeng.upatras.gr
* Correspondence: akokka@tuc.gr (A.K.); ppanagiotopoulou@tuc.gr (P.P.)

Abstract: The oxidative dehydrogenation of propane with CO_2 (CO_2-ODP) was investigated over different metal oxides M_xO_y (M: Ca, Sn, Cr, Ga) supported on a SiO_2 surface. Catalysts were characterized employing nitrogen adsorption/desorption, X-ray diffraction (XRD), CO_2 temperature programmed desorption (CO_2-TPD) and pyridine adsorption/desorption experiments in order to identify their physicochemical properties and correlate them with their activity and selectivity for the CO_2-ODP reaction. The effect of operating reaction conditions on catalytic performance was also examined, aiming to improve the propylene yield and suppress side reactions. Surface acidity and basicity were found to be affected by the nature of M_xO_y, which in turn affected the conversion of propane to propylene, which was in all cases higher compared to that of bare SiO_2. Propane conversion, reaction rate and selectivities towards propylene and carbon monoxide were maximized for the Ga- and Cr-containing catalysts characterized by moderate surface basicity, which were also able to limit the undesired reactions leading to ethylene and methane byproducts. High surface acidity was found to be beneficial for the CO_2-ODP reaction, which, however, should not be excessive to ensure high catalytic activity. The silica-supported Ga_2O_3 catalyst exhibited sufficient stability with time and better than that of the most active Cr_2O_3-SiO_2 catalyst. Decreasing the weight gas hourly space velocity resulted in a significant improvement in both propane conversion and propylene yield as well as a suppression of undesired product formation. Increasing CO_2 concentration in the feed did not practically affect propane conversion, while led to a decrease in propylene yield. The ratio of propylene to ethylene selectivity was optimized for CO_2:C_3H_8 = 5:1 and space velocity of 6000 mL g^{-1} h^{-1}, most possibly due to facilitation of the C–H bond cleavage against that of the C–C bond. Results of the present study provided evidence that the efficient conversion of propane to propylene is feasible over silica-based composite metal oxides, provided that catalyst characteristics have been optimized and reaction conditions have been properly selected.

Keywords: CO_2-assisted oxidative dehydrogenation of propane; propylene production; RWGS; surface basicity/acidity; silica-supported catalysts; Ca; Sn; Cr; Ga; WGHSV; CO_2:C_3H_8 molar ratio

Citation: Florou, A.; Kokka, A.; Bampos, G.; Panagiotopoulou, P. CO_2-Assisted Oxidative Dehydrogenation of Propane to Propylene over Modified SiO_2 Based Catalysts. *Catalysts* **2024**, *14*, 933. https://doi.org/10.3390/catal14120933

Academic Editors: Xiujie Li and Guido Busca

Received: 9 November 2024
Revised: 11 December 2024
Accepted: 16 December 2024
Published: 18 December 2024

Correction Statement: This article has been republished with a minor change. The change does not affect the scientific content of the article and further details are available within the backmatter of the website version of this article.

1. Introduction

Propylene (C_3H_6) is one of the most important building blocks in the petrochemical industry, as it is essential for the production of a wide range of chemicals such as polypropylene, acrylonitrile and propylene oxide [1–4]. Traditionally, C_3H_6 is produced via fluid catalytic cracking and steam cracking of naphtha and oil-based feedstocks, where it is produced as a by-product [1,4,5]. However, as the global demand for C_3H_6 continues to rise, these traditional production methods are inadequate to meet the aforementioned growing needs due to their low efficiency in producing C_3H_6 as well as the fast depletion of fossil fuel resources [1].

In recent years, dehydrogenation of propane (DP) (1) has become an emerging method for producing C_3H_6 [1,3,6,7]. This is due to the development of hydraulic fracturing and

the rapid expansion of the shale gas industry, which enable the cost-effective extraction of large quantities of shale gas rich in propane (C_3H_8) [6]. However, the DP reaction is endothermic and thus requires high reaction temperatures in order to achieve high C_3H_6 yields [2,4,8]. Nevertheless, high temperatures may promote undesirable reactions such as thermal cracking, leading to the production of lighter alkanes and carbon, which can cause rapid catalyst deactivation [2–4].

$$C_3H_8 \leftrightarrow C_3H_6 + H_2 \qquad \Delta H^0_{298K} = 124.3 kJ/mol \tag{1}$$

Compared to the endothermic DP process, the oxidative dehydrogenation of C_3H_8 (ODP) is more attractive because its exothermic nature enables its conduction at lower temperatures, thus avoiding the drawbacks of the DP process [1,2]. In addition to the use of conventional oxygen (O_2) as the oxidizing agent, other mild oxidants such as carbon dioxide (CO_2), nitrous oxide (N_2O), sulfur-containing compounds, and halogens have also been proposed for the ODP reaction [2,9]. Among them, CO_2-assisted dehydrogenation of C_3H_8 (CO_2-ODP) (2) has recently gained interest as an efficient and eco-friendly process because it not only produces propylene but also utilizes the CO_2 emissions, thus contributing to the mitigation of the greenhouse effect [8,10,11]. Furthermore, adding CO_2 in the gas stream can shift the equilibrium towards C_3H_6 production by consuming the produced H_2 via the Reverse Water-Gas Shift (3) reaction, while it simultaneously can inhibit coke deposition by promoting the reverse Boudouard reaction (4), thus preventing catalyst deactivation [2,3,9,10,12].

$$CO_2 + C_3H_8 \leftrightarrow C_3H_6 + CO + H_2O \qquad \Delta H^0_{298K} = 165.4\ kJ/mol \tag{2}$$

$$CO_2 + H_2 \leftrightarrow CO + H_2O \qquad \Delta H^0_{298K} = 41.1\ kJ/mol \tag{3}$$

$$CO_2 + C \leftrightarrow 2CO \qquad \Delta H^0_{298K} = 172.4\ kJ/mol \tag{4}$$

Metal oxides such as CrO_x, VO_x, GaO_x and InO_x dispersed on the surface of SiO_2 and Al_2O_3 supports have been found to catalyze effectively the CO_2-ODP reaction [2,3,6,9–16]. Catalytic activity is significantly influenced by the catalyst's composition and physicochemical characteristics such as metal oxide loading, reducibility and basic/acidic properties. In particular, Xu et al. [13], who studied the effect of the support nature on catalytic activity of gallium-based catalysts, found that Ga_2O_3-Al_2O_3 exhibited higher catalytic activity compared to Ga_2O_3-SiO_2 due to the abundance of medium-strong acidic sites on alumina surface. In addition, Chen et al. [17] reported that the superior catalytic performance of In_2O_3-Al_2O_3 catalyst compared to In_2O_3-ZrO_2 and In_2O_3-SiO_2 for the CO_2-ODP reaction was mainly due to a combined effect of high In_2O_3 dispersion and balanced acid/base properties. Furthermore, CrO_x-SiO_2 catalyst prepared by the atomic layer deposition method was found to exhibit higher CrO_x particle dispersion and higher content of polychromate species than the impregnated one, leading to increased acidity, reducibility, and thus improved activity for the CO_2-ODP reaction [12].

Although some of the catalysts investigated so far were found to exhibit high ODP activity, they do not seem to fulfill criteria related to selectivity and long-term stability. In certain cases, the formation of coke, which has a significant impact on the life-time of the catalyst, cannot be suppressed, resulting in progressive catalyst deactivation [2,3,10–16,18,19]. Efforts in the suppression of side reactions so as to achieve high propylene yields and avoid catalyst deactivation have been focused on the optimization of operating reaction conditions that are generally related to operating temperature, contact time, and CO_2/C_3H_8 molar ratio as well as reactor configuration. Appropriate selection of reaction conditions also reduces the process energy required and therefore decreases the cost of industrial propylene production. Although the kinetics are more favorable at high temperatures, low temperatures are preferable in order to achieve high selectivities towards C_3H_6 [9]. High reaction temperatures favor both C–H and C–C bond cleavage, leading on the one hand to the propane conversion to propylene and on the other hand to side reactions such as

the conversion of propane towards methane (CH_4) and ethylene (C_2H_4) or carbon, and the propane hydrogenolysis yielding ethane (C_2H_6) and methane [18,20]. Moreover, it has been found that increasing the contact time of the reaction mixture with the catalyst surface can lead to an increase in both C_3H_8 conversion and C_3H_6 yield [21]. Michorczyk et al. [22] reported that increasing the W/F led to an increase in C_3H_6 yield over CrO_x-SiO_2 catalyst, while C_3H_6 selectivity generally remained constant and slightly decreased for W/F values higher than 40 g h mol^{-1}.

In addition to temperature and contact time, the partial pressure of CO_2 is essential for the CO_2-ODP process. As a general trend, C_3H_8 conversion increases with increasing CO_2 concentration in the gas stream, accompanied by a parallel enhancement of CO and H_2O formation as well as reduction of H_2 production [23]. Based on thermodynamics, the effect of the CO_2 and C_3H_8 concentration in the feed on the equilibrium CO/H_2 molar ratio produced is significantly higher compared to the effect of temperature. Higher CO/H_2 molar ratios can be achieved for CO_2/C_3H_8 molar ratios higher than one. However, the influence of CO_2 partial pressure on the overall efficiency of the process depends strongly on the type of catalyst employed. In this respect, both a positive and a negative role of CO_2 have been suggested [24]. According to the positive role, as mentioned above, CO_2 facilitates (a) the transformation of H_2 to CO and H_2O through the RWGS reaction and (b) the coke gasification via the reverse Boudouard reaction. The negative role of CO_2 involves blocking of the dissociative adsorption of propane on the catalyst surface and is more evident for high concentrations of CO_2, which, as an acidic compound, competes with hydrogen ions abstracted from propane for the same basic adsorption sites on the catalyst surface. Concerning reactor configuration, the use of membrane reactors has been recently proposed to be beneficial for ODP with CO_2, by shifting the equilibrium towards production of pure propylene [18,25].

In our previous study, it was found that the addition of metal oxides (10%M_xO_y, M: Ce, Zr, Ca, Cr, Ga) on TiO_2 surface was able to improve catalytic performance for the CO_2-assisted oxidative dehydrogenation of propane due to a synergetic interaction between M_xO_y and the TiO_2 support, which led to modification of the physicochemical properties of TiO_2, including the surface acidity/basicity, reducibility, and anatase/rutile ratio and the primary crystallite size of TiO_2 support. Optimum results were obtained over Cr_2O_3-TiO_2 and Ga_2O_3-TiO_2 catalysts, which both exhibited a three-fold higher propylene yield ($Y_{C_3H_6}$) compared to bare TiO_2. In order to examine whether a similar improvement can be achieved in the catalytic activity of silica-supported catalysts, herein, we study the addition of various M_xO_y (M: Ca, Sn, Cr, Ga) on SiO_2 surface for the production of propylene via the CO_2-ODP reaction. An attempt was made to optimize the operating parameters (temperature, space velocity and CO_2:C_3H_8 molar ratio) in order to increase the process efficiency.

The main new findings of the present study lie in the following key points: (a) remarkable volcano type and inverse volcano type correlations between the process efficiency (propane conversion, reaction rate and product selectivity) and the surface acidity/basicity of the modified SiO_2 catalysts, which may be useful for designing catalysts suitable for the CO_2-ODP reaction, which, nowadays, is considered a promising approach for the on-purpose propylene production; (b) development of stable catalysts for the CO_2-ODP reaction, which is of significant practical importance since, according to numerous previous studies, catalyst deactivation is the main drawback of this process; (c) optimization of operating reaction conditions with respect to catalytic activity as well as propylene selectivity against side product selectivity, aiming to increase the conversion of propane towards propylene.

2. Results and Discussion

2.1. Catalyst Characterization

Results of nitrogen physisorption measurements obtained over the bare SiO_2 and M_xO_y-SiO_2 catalysts are summarized in Table 1. As can be seen, the specific surface area (SSA) of the bare SiO_2 was found to be 222.1 m^2 g^{-1}. The dispersion of M_xO_y on SiO_2 surface resulted in materials with lower SSA compared to that of the bare SiO_2 sample, ranging from 109.9 m^2 g^{-1} for CaO-SiO_2 to 220.9 m^2 g^{-1} for Cr_2O_3-SiO_2. A corresponding decrease in the SSA was also reported in previous studies over composite metal oxides, which was attributed to the partial blockage of the parent material pores (in our case, the SiO_2 sample) caused by the presence of M_xO_y on its surface [26–31]. Blocking of silica pores by the M_xO_y addition may be also responsible for the lower pore volume measured over CaO-SiO_2 (0.047 cm^3 g^{-1}), Ga_2O_3-SiO_2 (0.091 cm^3 g^{-1}) and SnO_2-SiO_2 (0.104 cm^3 g^{-1}) compared to bare SiO_2 (1.266 cm^3 g^{-1}) (Table 1) [30,31]. Interestingly, a higher pore volume was found for Cr_2O_3-SiO_2 (1.435 cm^3 g^{-1}), which was previously correlated with the additional porosity of the larger M_xO_y particles that interact more weakly with the support [11].

Table 1. Physicochemical characteristics of SiO_2 and 10%M_xO_y-SiO_2 catalysts.

Catalyst	SSA (m^2 g^{-1})	Pore Volume (cm^3 g^{-1})
SiO_2	222.1	1.266
10%SnO_2-SiO_2	196.5	0.104
10%Ga_2O_3-SiO_2	183.3	0.091
10%Cr_2O_3-SiO_2	220.9	1.435
10%CaO-SiO_2	109.9	0.047

The XRD patterns of the synthesized SiO_2 and M_xO_y-SiO_2 catalysts are shown in Figure S1. Results indicated that, in most cases, no sharp peaks attributed to SiO_2 were detected in the obtained diffractograms. The presence of SiO_2 was confirmed by a relatively broad peak located at 23.59° attributed to (2 0 1) reflection of tetragonal SiO_2 (JCPDS Card No. 32-993). No diffraction peaks assigned to Ga_2O_3 or CaO were discerned over Ga_2O_3-SiO_2 (trace c) and CaO-SiO_2 (trace d), indicating that Ga_2O_3 and CaO were well dispersed on silica surface and/or characterized by low crystallinity, in agreement with previous studies [2,26,27]. On the other hand, in the case of the Cr_2O_3-SiO_2 (trace b) sample, besides the broad band at 23.59°, peaks located at 2θ equal to 24.55°, 33.57°, 36.39°, 41.58°, 50.40° and 54.99° assigned to (0 1 2), (1 0 4), (1 1 0), (1 1 3), (0 2 4) and (1 1 6) planes of rhombohedral Cr_2O_3 (JCPDS Card No. 1-1294) were detected. Similarly, crystallographic peaks located at 26.72°, 38.11°, 52.22°, 54.99°, 58.37°, 62.30°, 64.72° and 71.47° attributed to (1 1 0), (2 0 0), (2 1 1), (2 2 0), (0 0 2), (3 1 0), (1 1 2) and (2 0 2) facets of tetragonal SnO_2 (JCPDS Card No. 1-657) were observed in the XRD pattern of SnO_2-SiO_2 (trace e) catalyst. The mean crystallite sizes of Cr_2O_3 and SnO_2 were estimated using the Scherrer's equation [26] and found to be 19.9 and 10 nm, respectively.

The surface basicity of the investigated SiO_2 and M_xO_y-SiO_2 catalysts was studied by conducting CO_2-TPD experiments. Results obtained following 5%CO_2/He adsorption at 25 °C for 30 min and, then, 30 min purging under He flow are presented in Figure 1. It was observed that in all cases, two CO_2 desorption peaks were evolved: a low temperature (LT) peak centered at ca. 99–105 °C due to CO_2 desorption from weak basic sites [32–36], and a high temperature (HT) peak appearing above 500 °C that could be assigned to CO_2 desorption from strong basic sites [34,36–38]. The position of the LT peak was not affected by the presence and/or type of M_xO_y on SiO_2 surface, contrary to the HT peak, which was shifted towards lower temperatures (by ~77 °C) following the order Cr_2O_3~Ga_2O_3~(bare) SiO_2 < SnO_2 < CaO. This implies that the strength of weak basic sites was not, practically, affected by the presence of M_xO_y on SiO_2 surface, whereas that of strong basic sites was varied depending on the type of M_xO_y. An additional weak peak was detected at higher

temperatures (~715 °C) over the CaO-containing catalyst, indicating that the population of strong basic sites was higher over this sample, in agreement with previous studies [26,39].

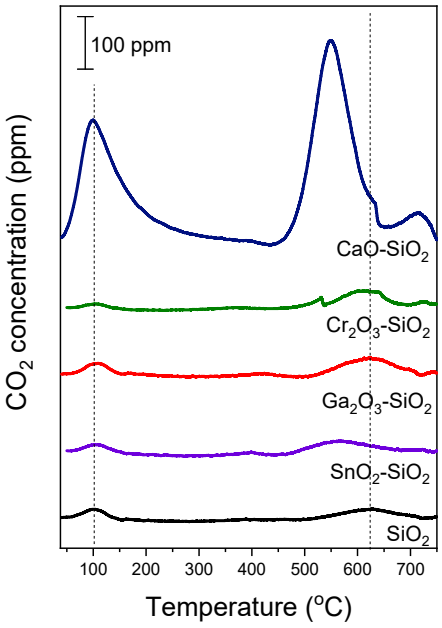

Figure 1. CO_2-TPD profiles obtained from SiO_2-based catalysts. Experimental conditions: mass of catalyst: 0.15 g; heating rate β = 10 °C /min; total flow = 40 cm^3 min^{-1}.

Integrating the area below the LT and HT peak enabled the estimation of the amount (in μmol g^{-1}) of CO_2 desorbed from the weak and strong basic sites, respectively (Table S1). In an attempt to eliminate the factor attributed to the SSA of the investigated catalysts, which significantly varied from 109.9 to 222.1 m^2 g^{-1} (Table 1), the estimated values of desorbed CO_2 were divided by the corresponding values of the SSA, and the resulting amounts of CO_2 desorbed in μmol m^{-2} are presented in Table 2. As can be seen, the amount of CO_2 desorbed at low temperatures increased from 0.003 to 0.162 μmol m^{-2} in the order Cr_2O_3 < (bare) SiO_2 ~ SnO_2 ~ Ga_2O_3 << CaO, while that at high temperatures increased from 0.018 to 0.663 μmol m^{-2} in the order (bare) SiO_2 < SnO_2 < Ga_2O_3 ~ Cr_2O_3 << CaO. Results indicated that the population of weak basic sites was not affected by the addition of SnO_2 and Ga_2O_3 on silica surface, was decreased in the presence of Cr_2O_3, and was remarkably increased for the CaO-containing catalyst. On the other hand, the induced effect of M_xO_y addition on the population of strong basic sites was higher than that of weak basic sites, and was in all cases enhanced compared to bare SiO_2. Therefore, the total surface basicity was mainly determined by that of strong basic sites following the same order and was found to increase from 0.021 μmol m^{-2} for the bare SiO_2 to 0.825 μmol m^{-2} for the CaO-SiO_2 catalyst (Table 2).

Table 2. Amount of desorbed CO_2 during CO_2-TPD experiments.

Catalyst	LT Peak (μmol m^{-2})	HT Peak (μmol m^{-2})	Total Amount of Desorbed CO_2 (μmol m^{-2})
SiO_2	0.003	0.018	0.021
10%SnO_2-SiO_2	0.003	0.032	0.035
10%Ga_2O_3-SiO_2	0.003	0.040	0.043
10%Cr_2O_3-SiO_2	0.001	0.042	0.043
10%CaO-SiO_2	0.162	0.663	0.825

The enhancement of surface basicity via modification of silica surface by CaO, Ga_2O_3, or Cr_2O_3 was also reported in previous studies [13,36,38]. For example, Al-Muhtaseb et al. [36], demonstrated that the addition of CaO on SiO_2 surface led to a significant increase in the number of both weak and strong basic sites, compared to those of pristine SiO_2, in excellent agreement with the results in Figure 1. Similarly, the amount of CO_2 desorbed from Ga_2O_3-SiO_2 surface during CO_2-TPD was found to be twice higher than that desorbed from pure SiO_2 surface [13]. Zăvoianu et al. [38] also found that doping with Cr enhanced the basic character of the silica-supported $NiMoO_4$ catalyst. Although no previous studies were reported (at least to our knowledge) related to the alteration of basic properties of silica by tin oxide addition, SnO_2 was demonstrated to be able to increase the number and strength of strong basic sites when it was supported on ZrO_2 surface due to the synergistic effect between the two metal oxides [40].

Pyridine adsorption/desorption experiments combined with FTIR spectroscopy were also carried out to determine the nature and strength of surface acid sites of the synthesized catalysts. Results obtained are summarized in Figure 2 and Figure S2. In the case of bare SiO_2 catalyst (Figure 2a), the spectrum recorded at 25 °C (trace a) following pyridine adsorption at 25 °C for 2 h was characterized by two weak bands located at 1599 and 1448 cm^{-1} previously attributed to pyridine adsorbed on weak/moderate and strong Lewis acid sites, respectively [41–45]. Contributions by physisorbed pyridine may have also coexisted in the 1448 cm^{-1} band [41,43,44]. Progressive increase in temperature in He flow resulted in the disappearance of both bands above 150 °C, implying that they were weakly adsorbed on silica surface.

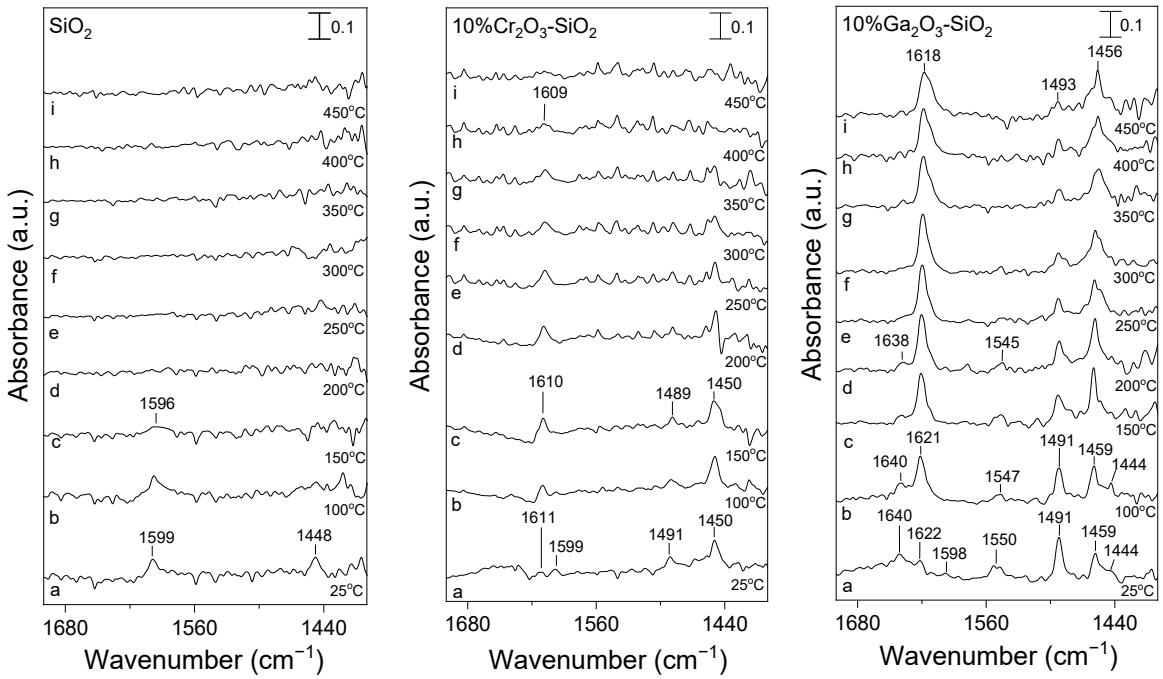

Figure 2. DRIFT spectra obtained from (**a**) SiO_2, (**b**) 10%Cr_2O_3-SiO_2 and (**c**) 10%Ga_2O_3-SiO_2 catalysts following adsorption of pyridine at 25 °C for 120 min and subsequent stepwise heating at the indicated temperatures under He flow (a: 25 °C; b: 100 °C; c: 150 °C; d: 200 °C; e: 250 °C; f: 300 °C; g: 350 °C; h: 400 °C; i: 450 °C).

The addition of SnO_2, Cr_2O_3 and Ga_2O_3 on SiO_2 led to the development of additional bands in the 1700–1400 cm^{-1} region in the corresponding obtained spectra. Specifically, in addition to the bands assigned to pyridine adsorption on Lewis acid sites (1598–1599 cm^{-1}, 1450–1453 cm^{-1}), the spectrum obtained at 25 °C from SnO_2-SiO_2 catalyst (Figure S2a,

trace a) consisted of two more bands, located at 1641 and 1493 cm^{-1}. The former band can be attributed to pyridine species interacting with Brønsted acid sites, while the later one was previously reported to reflect a mix of both Lewis and Bronsted acid sites [41,43,44,46–49]. A new shoulder was developed at ca. 1612 cm^{-1} by increasing temperature at 100 °C under He flow, which survived on the catalyst surface up to 250 °C (trace e) and was due to strong Lewis acid sites [41,42,44]. No band was detected above 250 °C, implying that all pyridine species were completely desorbed.

Adsorption of pyridine on Cr_2O_3-SiO_2 catalyst at 25 °C (Figure 2b, trace a) gave rise to three IR bands associated with Lewis acid sites (1611, 1599 and 1450 cm^{-1}) and the characteristic band at 1491 cm^{-1} associated with both Lewis and Brønsted acid sites [41,43,44,46–48,50]. Although most bands disappeared from the spectra obtained above 250 °C, the one detected at 1611 cm^{-1} could be discerned up to 400 °C, confirming the above suggestion that this band is related to strong Lewis acid sites. Interestingly, the population of adsorbed pyridine species was significantly higher over Ga_2O_3-SiO_2 (Figure 2c) catalyst in the entire temperature range examined. Bands owing to (a) pyridine adsorption on strong and weak/moderate Lewis acid sites (1622, 1598, 1491 and 1459 cm^{-1}), (b) pyridine protonated by Brønsted acid sites (1640, 1550 and 1491 cm^{-1}) and (c) physisorbed pyridine (1444 cm^{-1}) were present in the spectrum collected at 25 °C [14,41–44,49,51]. Heating of catalyst in He flow resulted in an increase in the relative intensity of bands attributed to strong Lewis acid sites (1622 and 1459 cm^{-1}) that were present in the spectra obtained up to 450 °C (trace i), implying that the corresponding species were thermally stable. This was also the case for the characteristic band containing contributions from both Lewis and Brønsted acid sites (1491 cm^{-1}), which, although, decreased in intensity, could be clearly observed at temperatures as high as 450 °C (trace i). In contrast, pyridine species associated with Brønsted acid sites could not be discerned above 300 °C (trace f), while the band due to a weak/moderate Lewis acid site (1598 cm^{-1}) disappeared already at 100 °C (trace b).

Regarding the spectra obtained from CaO-SiO_2 catalyst (Figure S2b), no bands were detected in the whole temperature range investigated, indicating the absence of acid sites on the surface of this catalyst. This is consistent with the results of Torres et al. [45], who found that the addition of CaO on Al_2O_3 surface reduced its acidic character, leading to the absence of IR bands in its spectrum.

Comparison between the investigated catalysts showed that the addition of M_xO_y on SiO_2 surface strongly affects the nature, the population and the strength of acid sites. Evidence was provided that the surface acidity follows the order CaO-SiO_2 << SiO_2 < SnO_2-SiO_2 < Cr_2O_3-SiO_2 < Ga_2O_3-SiO_2. Results are in agreement with our previous study of M_xO_y-TiO_2 catalysts, where it was found that the surface acidity of TiO_2 was slightly increased by Cr_2O_3 addition, while it was significantly enhanced in the presence of Ga_2O_3 additive [26].

2.2. Catalytic Performance of M_xO_y-SiO_2 Catalysts

Results of catalytic performance tests obtained over SiO_2 supported metal oxides and bare SiO_2 for the CO_2-assisted oxidative dehydrogenation of propane are presented in Figure 3. Experiments were carried out using a CO_2:C_3H_8 molar ratio of 5:1 (5% C_3H_8 + 25% CO_2/He) and a WGHSV of 6000 mL g^{-1} h^{-1}. As was observed, propane conversion ($X_{C_3H_8}$) measured for bare SiO_2 support progressively increased from 1.2 to 58% as the reaction temperature increased from 610 to 740 °C (Figure 3a). The propane conversion curve was shifted towards lower reaction temperatures with the addition of 10 wt.% M_xO_y (M: Ga, Cr, Ca, Sn) on SiO_2 surface. This shift was more notable for the Cr_2O_3-containing catalyst (by ~110 °C for $X_{C_3H_8}$ = 30%) and milder for the Ga_2O_3-, CaO- and SnO_2-containing samples (by ~30 °C for $X_{C_3H_8}$ = 30%). Specifically, the most active Cr_2O_3-SiO_2 catalyst was activated at ~480 °C and achieved a $X_{C_3H_8}$ of approximately 77% at 740 °C. The Ga_2O_3-SiO_2 and CaO-SiO_2 catalysts exhibited intermediate and similar performance. Although the SnO_2-SiO_2 catalyst was activated at temperatures similar to those of the bare SiO_2 support,

it was able to achieve $X_{C_3H_8}$ comparable to those measured for Ga_2O_3- and CaO-containing samples at temperatures higher than 650 °C, reaching $X_{C_3H_8}$ of 72% at 740 °C.

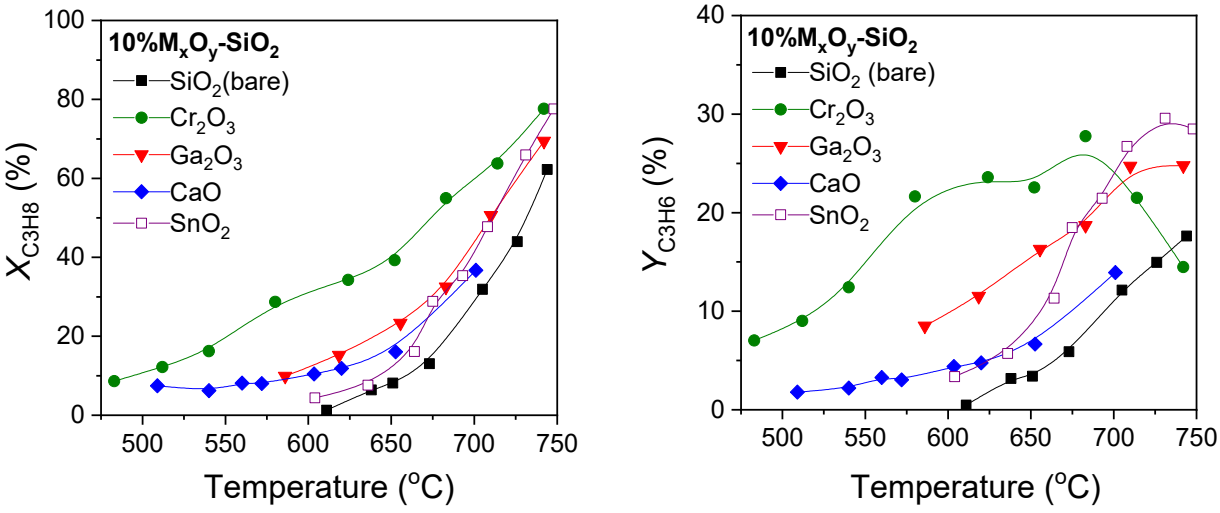

Figure 3. Effect of reaction temperature on the (**a**) conversion of propane and (**b**) propylene yield obtained over SiO_2 and 10%M_xO_y-SiO_2 catalysts. Experimental conditions: particle diameter: $0.15 < d_p < 0.25$ mm; CO_2:C_3H_8 = 5:1; WGHSV = 6000 h^{-1}.

A remarkable increase was also observed in propylene yield with the addition of metal oxides on SiO_2 surface, which seems to depend on both the type of M_xO_y and the reaction temperature (Figure 3b). In particular, $Y_{C_3H_6}$ at 610 °C increased from 0.6 to 23% following the order (bare) SiO_2 < SnO_2-SiO_2~CaO-SiO_2 < Ga_2O_3-SiO_2 < Cr_2O_3-SiO_2. However, at higher temperatures, $Y_{C_3H_6}$ was found to be significantly higher for SnO_2-SiO_2 compared to CaO-SiO_2 and comparable to or even higher than that for Ga_2O_3-SiO_2 (for T > 675 °C). Although, Cr_2O_3-SiO_2 exhibited superior values of $Y_{C_3H_6}$ up to 683 °C compared to the other catalysts, its value notably dropped from 28 to 15% as the temperature was raised from 683 to 740 °C.

The variation in product selectivity with temperature for the investigated metal oxides is presented in Figure 4. Propylene, carbon monoxide, methane, ethylene and traces of ethane were detected for all the examined catalysts. In the case of bare SiO_2 (Figure 4a), the selectivity towards C_3H_6 ($S_{C_3H_6}$) was slightly increased from 38 to 50% upon increasing temperature from 610 to 638 °C, but it was significantly reduced to 29% with a further increase in temperature to 740 °C. Carbon monoxide production implies that the desired reactions of oxidative dehydrogenation of propane with CO_2 (2) and RWGS (3) were operable under the present experimental conditions, whereas part of CO may be also produced via the reverse Boudouard reaction (4). However, the selectivity towards CO (S_{CO}) was generally low and decreased from 7.6 to 0.3% in the temperature range of 610–740 °C. This indicates that the CO_2-ODP reaction was probably limited and that the direct dehydrogenation of propane prevailed above 670 °C, where S_{CO} was lower than 1%. The selectivities towards CH_4 (S_{CH_4}), and C_2H_4 ($S_{C_2H_4}$) were generally high and increased slightly from 18 to 23% and from 35 to 46%, respectively, with increasing temperature from 610 to 740 °C. A small increase was also observed for the C_2H_6 selectivity ($S_{C_2H_6}$), which was always lower than 1.3% under the present experimental conditions. Results imply that the C_3H_8 hydrogenolysis as well as the C_3H_8 and/or C_3H_6 decomposition were favored at high reaction temperatures, in agreement with previous studies [2,26,52].

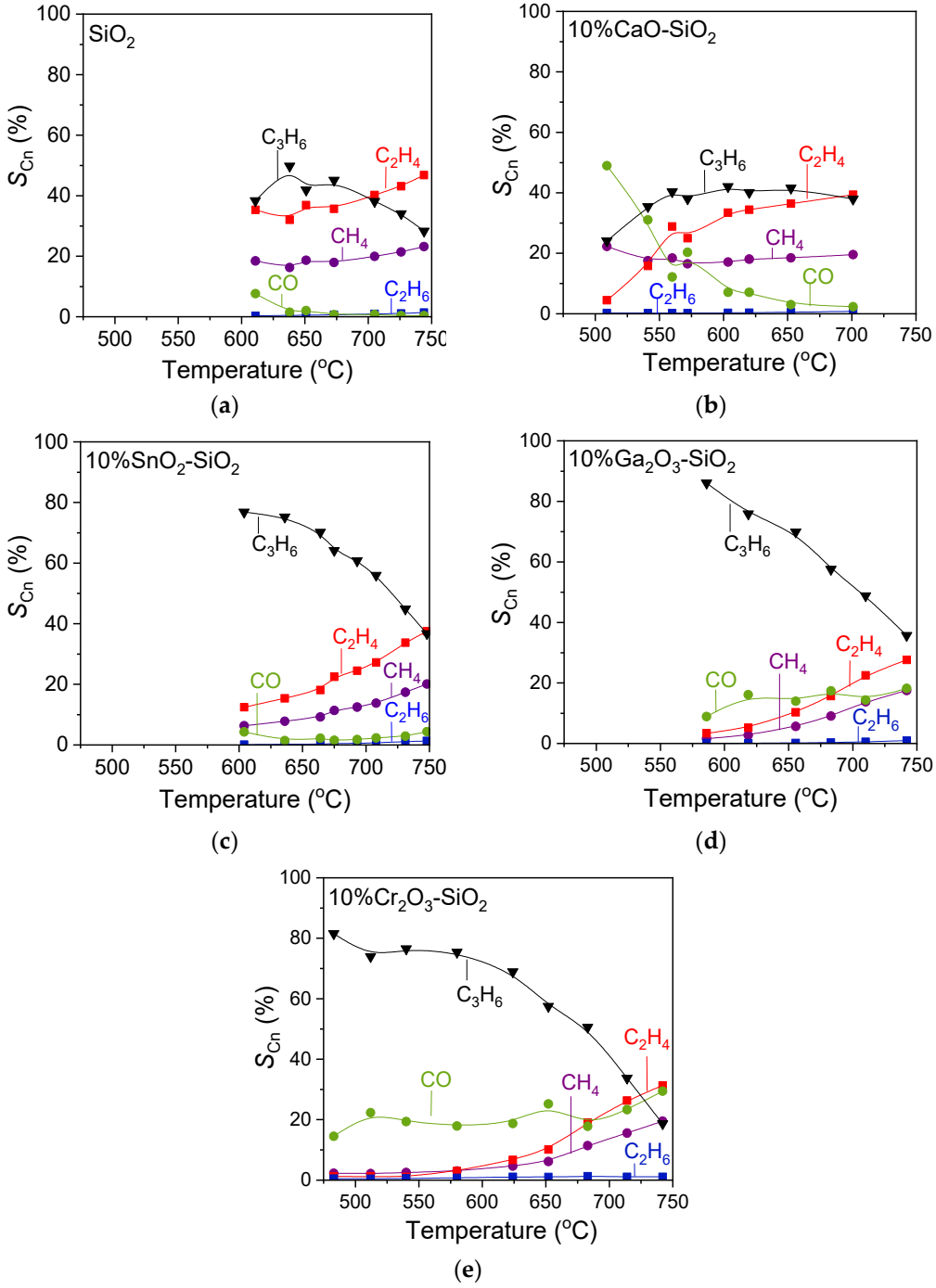

Figure 4. Selectivities towards reaction products as a function of reaction temperature obtained over (**a**) SiO_2, (**b**) 10%CaO-SiO_2, (**c**) 10%SnO_2-SiO_2, (**d**) 10%Ga_2O_3-SiO_2 and (**e**) 10%Cr_2O_3-SiO_2 catalysts. Experimental conditions: same as in Figure 3.

Product distribution with temperature was significantly modified over the M_xO_y-SiO_2 catalysts (Figure 4b–e). With the exception of the CaO-SiO_2 sample, which exhibited $S_{C_3H_6}$ comparable to that of bare SiO_2, propylene selectivity was remarkably higher for the rest of the composite metal oxides, especially for Ga_2O_3-SiO_2 and Cr_2O_3-SiO_2, where $S_{C_3H_6}$ reached 86% at 586 °C and 81.5% at 483 °C, respectively. Although CaO deposition on SiO_2 surface did not influence $S_{C_3H_6}$, S_{CO} was found to be significantly enhanced in the presence of CaO ($S_{CO} > S_{C_3H_6}$ below 535 °C), indicating that the RWGS and/or reverse Boudouard reactions may dominate over this catalyst against the CO_2-ODP reaction, resulting in higher production of CO, in agreement with previous studies [26,53]. In contrast, S_{CO}

was limited (<4.3%) for the SnO_2-SiO_2 catalyst, whereas it remained practically constant for the Ga_2O_3-SiO_2 (~17%) and Cr_2O_3-SiO_2 (~19%) samples below 700 °C and increased slightly at higher temperatures. It is of interest to note that S_{CH_4} and $S_{C_2H_4}$, measured for SnO_2-SiO_2, Ga_2O_3-SiO_2 and Cr_2O_3-SiO_2 catalysts, were significantly lower compared to those measured for pure SiO_2 and CaO-SiO_2 samples in the entire temperature range examined. This indicates that undesired reactions were mitigated to some extent over the former samples and, in fact, were practically suppressed below 625 °C for the Ga_2O_3-SiO_2 and Cr_2O_3-SiO_2 catalysts. Ethylene was, in all cases, produced in trace amounts (<1.3%).

Results of the present study are in agreement with those reported by Takehira et al. [54], who found that Cr-MCM-41 catalyst exhibited higher catalytic performance compared with Ga-MCM-41 catalyst for the oxidative dehydrogenation of propane with CO_2. Chromium-based catalysts are generally considered to be among the most active catalysts for the CO_2-ODP reaction [1,18]. Their high catalytic performance has been attributed to their distinct oxidation states and redox properties, which are depended on the loading and dispersion of chromium species as well as the nature of the support employed [1,18,55]. In our previous study, it was found that the addition of M_xO_y (M: Zr, Ce, Ca, Cr, Ga) on TiO_2 surface resulted in an improvement of propane conversion and propylene yield, with the Cr_2O_3- and Ga_2O_3-TiO_2 catalysts exhibiting optimum performance [26]. The improved catalytic performance was attributed to a synergetic interaction between M_xO_y and TiO_2 support that led to modification of the physicochemical properties of TiO_2, including the surface acidity/basicity, the reducibility, and the anatase/rutile ratio and mean crystallite size of TiO_2 support. Among the above catalyst characteristics, surface basicity was found to play a key role in the CO_2-ODP process. In particular, it was demonstrated that catalytic performance was increased with increasing surface basicity, which was maximized for the Cr_2O_3- and Ga_2O_3-containing samples, while it was notably decreased for the highly basic CaO-TiO_2 catalyst.

Based on the results shown in Figures 1, 3 and 4, a similar trend was found to be followed for the M_xO_y-SiO_2 catalysts of the present study. This can be clearly seen in Figure 5, where the propane conversion, the reaction rate normalized with respect to the SSA ($r_{C_3H_8}$, in μmol m^{-2}), and the selectivities towards reaction products measured at 610 °C are plotted as a function of the total amount of desorbed CO_2 during CO_2-TPD experiments for all the investigated catalysts. As can be seen, both the propane conversion and the reaction rate increased with increasing surface basicity, taking a maximum value for the Cr_2O_3-SiO_2 catalyst, and then decreased for the CaO-SiO_2 sample, which exhibited significantly higher surface basicity (Figure 5). It is of interest to note that, although the Ga_2O_3-SiO_2 catalyst exhibited surface basicity similar to that of Cr_2O_3-SiO_2 catalyst, its propane conversion and reaction rate were lower. This may imply that additional physicochemical characteristics also affect the rate of C_3H_8 conversion to C_3H_6. Selectivities towards C_3H_6 and CO followed the same trend with that of reaction rate, i.e., they presented a maximum value for the samples characterized by moderate surface basicity (Figure 5). Specifically, Ga_2O_3-SiO_2 catalyst was the most selective towards propylene, whereas Cr_2O_3-SiO_2 catalyst was the most selective towards CO. On the other hand, S_{CH_4} and $S_{C_2H_x}$ went through a minimum value for the Ga_2O_3-SiO_2 and Cr_2O_3-SiO_2 catalysts (Figure 5), indicating that moderate surface basicity led to elimination of the undesired reactions.

Apart from surface basicity, catalytic performance seemed to be influenced by surface acidity and generally enhanced for the samples characterized by a higher number and strength of acid sites on the catalyst surface. Comparison between results in Figures 2 and 4 clearly demonstrates that the catalyst ranking with respect to $S_{C_3H_6}$ was roughly similar to that obtained with respect to surface acidity. It should be noted, however, that the lower propane conversion and reaction rate obtained for the Ga_2O_3-containing sample compared with that containing Cr_2O_3 may be due to the higher surface acidity of the former sample, as evidenced by DRIFTS results in Figure 2. This implies that, similarly to surface basicity, surface acidity should not exceed an optimum value in order for the catalyst to be able to selectively convert propane to propylene.

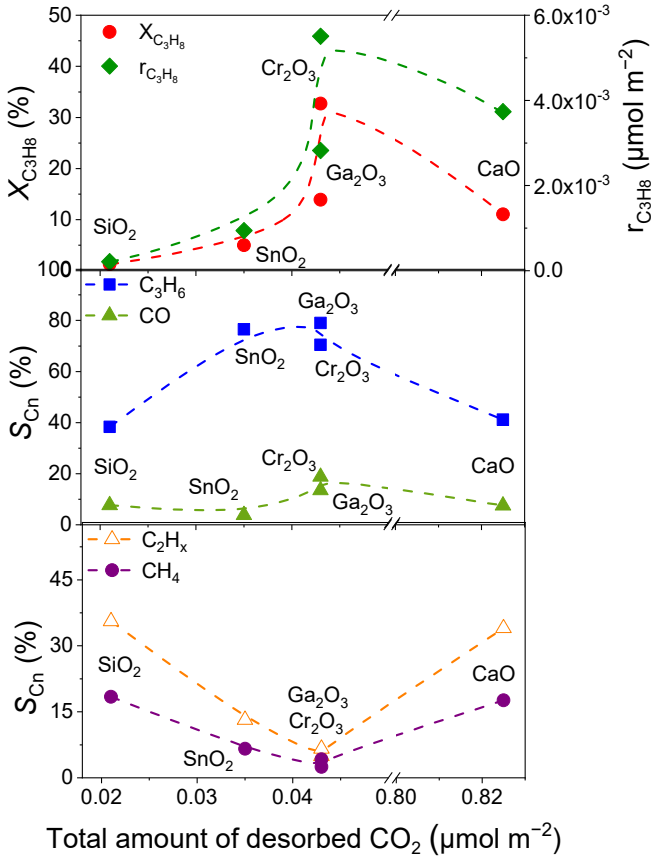

Figure 5. Propane conversion, reaction rate and product selectivities at 610 °C as a function of the total amount of desorbed CO_2 during CO_2-TPD experiments for SiO_2 and 10%M_xO_y-SiO_2 catalysts.

The induced effect of the number and strength of catalyst acid sites on the catalytic performance for the CO_2-assisted oxidative dehydrogenation of propane was also reported in previous studies. For example, Wang et al. [56] investigated the performance of various CrO_x-doped mesoporous silica spheres and found that catalytic activity was optimized for the sample exhibiting the highest proportion of medium acid sites. In addition, Daresibi et al. [12] reported that highly dispersed CrO_x particles on SiO_2 characterized by higher density of polychromate species resulted in higher surface acidity and catalytic activity for the CO_2-ODP reaction. Furthermore, Tedeeva et al. [2] demonstrated that catalytic activity of Ga_2O_3 catalysts supported on various SiO_2 supports depended on both the gallium oxide loading and the textural characteristics of the support. According to the authors, high propane conversions and propylene selectivities could be achieved over well-dispersed Ga_2O_3 particles on a support surface that was characterized by a high specific surface area and number of acid sites. Similarly, we recently reported that the nature of the support strongly influences both the catalytic activity and surface acidity of gallium oxide-based catalysts [52]. Moreover, in our previous study, it was found that although the Cr_2O_3-TiO_2 and Ga_2O_3-TiO_2 catalysts exhibited remarkably higher and similar catalytic activity compared to bare TiO_2, the Cr_2O_3-TiO_2 and TiO_2 catalysts presented similar surface acidity notably lower than that of Ga_2O_3-TiO_2, suggesting that surface acidity influenced catalytic performance, but it was not the only factor affecting it [26].

Based on the XRD results (Figure S1) discussed above, no diffraction peaks assigned to Ga_2O_3 or CaO were discerned over Ga_2O_3-SiO_2 and CaO-SiO_2 catalysts, indicating that Ga_2O_3 and CaO were well dispersed on silica surface, contrary to Cr_2O_3-SiO_2 and SnO_2-SiO_2 catalysts where rhombohedral Cr_2O_3 and tetragonal SnO_2 structures were identified with a primary crystallite size of 19.9 and 10 nm, respectively. Taking into account the catalysts' rankings with respect to their activity for the CO_2-ODP reaction, no monotonous

trend seemed to exist between catalytic activity and the crystallite size of the metal oxide additive, implying that this parameter does not practically influence the CO_2-ODP process. This was also the case for the specific surface area and pore volume, since the most active Cr_2O_3-SiO_2 catalyst was found to be characterized by a similar specific surface area and slightly higher pore volume compared to the least active bare SiO_2.

It is worth noting that the results for both $X_{C_3H_8}$ and $S_{C_3H_6}$ achieved in the present study were comparable and in certain cases higher than those reported in previous works over silica-based catalysts, as depicted in Table 3. Better results have been achieved in terms of initial propane conversion over Cr(3%)O_x/KSKG [57], Ga(10%)O_x/Silica [57], 5CrO_x/silicalite-1 [58] and 10%Ga_2O_3-SiO_2 [59] catalysts, which, however, gradually decreased with time on stream and had not yet been stabilized when the experiment was stopped.

Regarding the stability of the catalysts investigated in the present work, time on stream (TOS) stability tests were carried out over the most active Cr_2O_3-SiO_2 and Ga_2O_3-SiO_2 catalysts at 660 °C. In these experiments, the catalyst remained under He flow every night after completion of 5–6 h interaction with the reaction mixture (as indicated with the dashed vertical lines). Results showed that Ga_2O_3-SiO_2 catalyst exhibited sufficient stability for 22 h on stream, with $X_{C_3H_8}$ and $S_{C_3H_6}$ taking values of 24–31% and 54.5–57%, respectively (Figure 6). The small decrease in $X_{C_3H_8}$ observed after the shutdown of the system overnight indicates that Ga_2O_3-SiO_2 catalyst lost part of its initial activity, which, however, could be regained following its exposure to the reaction mixture. Interestingly, selectivity towards C_3H_6 was not affected by this slight decrease in $X_{C_3H_8}$. Regarding Cr_2O_3-SiO_2 catalyst, a decrease in $X_{C_3H_8}$ from 58 to 40.5% was observed during the first 5 h on stream; this did not practically influence propylene selectivity, which varied between 49.2–50.5%. Further catalyst operation under CO_2-ODP conditions led to a smaller decrease in propane conversion, reaching 35%, which was followed by a slight decrease in $S_{C_3H_6}$ from 49 to 43.5% after ~20 h on stream. Since CO_2 was in excess concentration (25%), the conversion of CO_2 was generally low for both catalysts examined, taking slightly higher values (X_{CO_2} = 3.5–6.6%) for Cr_2O_3-SiO_2 compared to Ga_2O_3-SiO_2 (X_{CO_2} = 1.6–4.3%).

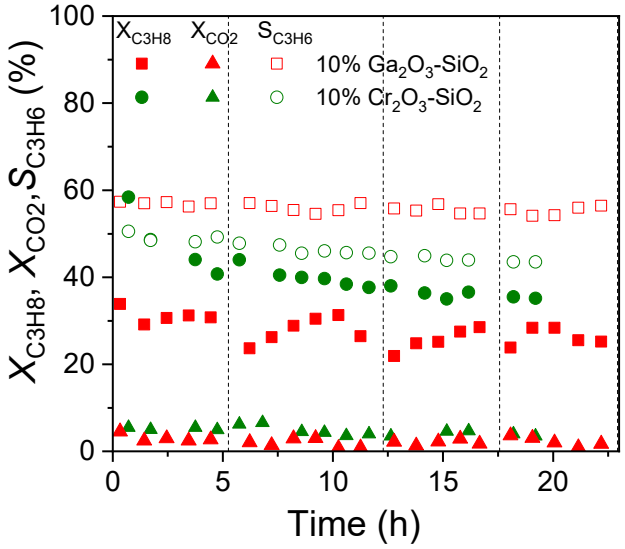

Figure 6. Effect of reaction time on the conversions of C_3H_8 and CO_2 (solid symbols), and selectivity towards C_3H_6 (open symbols) at 660 °C over 10%Cr_2O_3-SiO_2 and 10%Ga_2O_3-SiO_2 catalysts. Experimental conditions: same as in Figure 3.

Table 3. Comparison of results in the literature for the CO_2-ODP reaction.

Catalyst	CO_2-ODP Reaction Conditions (WGHSV; CO_2:C_3H_8 Ratio)	T (°C)	$X_{C_3H_8}$ (%)	$S_{C_3H_6}$ (%)	$Y_{C_3H_6}$ (%)	Ref.
10%Cr_2O_3-SiO_2	WGHSV = 6000 mL h^{-1} g^{-1} CO_2:C_3H_8 = 5:1	600	31.0 12.3	72 81.5	22.3 9.9	This work
10%Ga_2O_3-SiO_2	WGHSV = 3000 mL h^{-1} g^{-1} CO_2:C_3H_8 = 5:1	600	21.0	70.0	14.5	
5%Ga_2O_3-SiO_2	WGHSV = 6000 mL h^{-1} g^{-1} CO_2:C_3H_8 = 2:1	600	6.4	92	5.9	[13]
5%Cr_2O_3/SiO_2 5%Ga_2O_3/SiO_2	WGHSV = 3600 mL h^{-1} g^{-1} CO_2:C_3H_8 = 5:1	600	6.9 1.3	84 77.5	5.8 1.0	[60]
7Ga/SiO_2	WGHSV = 1800 mL h^{-1} g^{-1} CO_2:C_3H_8 = 2:1	600	21	81	17.0	[2]
CrO_x/SiO_2	WGHSV = 3600 mL h^{-1} g^{-1} CO_2:C_3H_8 = 7:1	600	36.3	92.4	33.5	[22]
Cr/MSS-2 [a]	WGHSV = 5400 mL h^{-1} g^{-1} CO_2:C_3H_8 = 4:1	600	32	89	28.5	[56]
Cr-MCM-41 Ga-MCM-41	WGHSV = 7504 mL h^{-1} g^{-1} CO_2:C_3H_8 = 5.6:1	550	17.0 5.0	93.5 96.0	16.0 5.0	[54]
Cr(3%)O_x/KSKG [b] Ga(10%)O_x/Silica	GHSV = 200 h^{-1} CO_2:C_3H_8 = 2:1	600	84.0 28.0	43.0 85.0	36.5 24.0	[57]
5CrO_x/silicalite-1	WGHSV = 3000 mL h^{-1} g^{-1} CO_2:C_3H_8 = 5:1	550	35.0	87.0	30.5	[58]
5Cr/SiO_2 5Cr/MCM-41	WGHSV = 1800 mL h^{-1} g^{-1} CO_2:C_3H_8 = 2:1	650	9.0 14.0	49.3 49.3	4.5 7.0	[31]
CrO_x/SiO_2	WGHSV = 4500 mL h^{-1} g^{-1} CO_2:C_3H_8 = 5:1	600	28.5	89.0	25.5	[12]
10%Ga_2O_3-SiO_2	WGHSV = 3900 mL h^{-1} g^{-1} CO_2:C_3H_8 = 1:1	600	37.0	91.5	33.9	[59]

[a] MMS: mesoporous silica spheres. [b] KSKG: silica gel of KSKG grade.

2.3. Effect of Weight Gas Hourly Space Velocity (WGHSV) on Catalytic Performance

Results presented in Figures 3–6 were obtained using a WGHSV of 6000 mL g^{-1} h^{-1}. In an attempt to optimize the operating reaction conditions, the effect of WGHSV on catalytic performance was investigated over the 10%Ga_2O_3-SiO_2 catalyst, which as shown above, was among catalysts exhibiting high activity and propylene selectivity as well as sufficient stability. In these experiments, the WGHSV was varied in the range of 3000–150,000 mL g^{-1} h^{-1} using a molar ratio of CO_2:C_3H_8 = 5. It should be mentioned that the WGHSV = 3000 mL g^{-1} h^{-1} was achieved using Ga_2O_3-SiO_2 catalyst in the form of pellets so as to reduce the catalyst volume and study the effect of space velocity over a wider range. Results obtained are shown in Figure 7 where the effect of WGHSV on the conversion of propane (Figure 7a) and propylene yield (Figure 7b) are plotted as a function of reaction temperature. It was observed that both the propane conversion and propylene yield curves were progressively shifted towards lower temperatures ($X_{C_3H_8}$ by ~93 °C and $Y_{C_3H_6}$ by ~137 °C) with decreasing WGHSV from 150,000 to 3000 mL g^{-1} h^{-1}. In particular, $X_{C_3H_8}$ and $Y_{C_3H_6}$ at 650 °C increased from 9 to 35% and from 4.5 to 18%, respectively, as WGHSV decreased from 150,000 to 3000 mL g^{-1} h^{-1}.

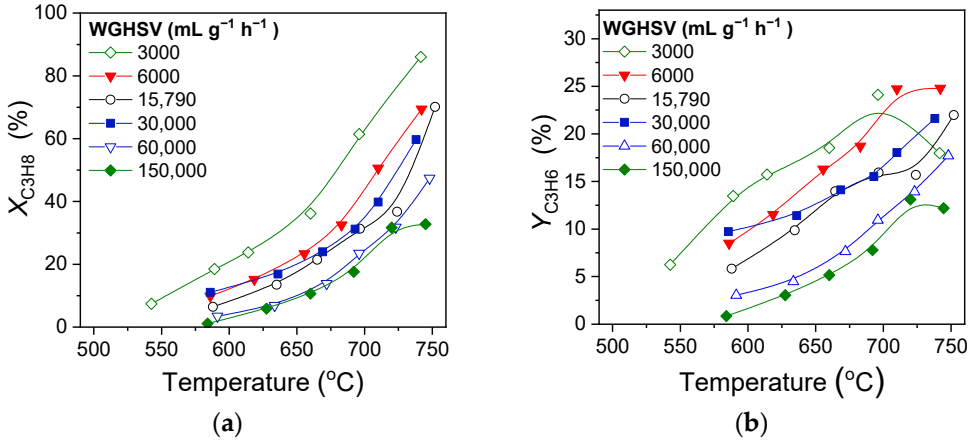

Figure 7. Effect of WGHSV on the (**a**) conversion of C_3H_8 and (**b**) yield of C_3H_6 over 10%Ga_2O_3-SiO_2 catalyst using a CO_2:C_3H_8 = 5:1.

Results of variation of product selectivities with temperature obtained for different space velocities (Figure S3) were qualitatively similar to those presented in Figure 4. In all cases, low reaction temperatures favored the oxidative dehydrogenation of propane, the RWGS and possibly the reverse Boudouard reactions, as evidenced by the high C_3H_6 selectivities and the production of CO. On the other hand, high reaction temperatures favored the undesired reactions of C_3H_8 hydrogenolysis and C_3H_8 and/or C_3H_6 decomposition yielding CH_4, C_2H_4 and traces of C_2H_6. Comparison between results obtained using different WGHSV showed certain quantitative differences that can be more clearly seen in Figure 8, where the effect of WGHSV on the selectivities towards reaction products at 600 and 700 °C are presented. In particular, a small increase in $S_{C_3H_6}$ from 70 to 86% was observed when increasing WGHSV from 3000 to 15,790 mL g^{-1} h^{-1}, respectively, at 600 °C, followed by a gradual decrease to 67.5% with further increase in WGHSV to 150,000 mL g^{-1} h^{-1} (Figure 8a). The increase in $S_{C_3H_6}$ in the WGHSV range of 3000–15,790 mL g^{-1} h^{-1} was accompanied by a decrease in S_{CH_4} and $S_{C_2H_4}$, which were minimized at 2.9 and 5.4%, respectively, for WGHSV = 6000 mL g^{-1} h^{-1}. However, the formation of both methane and ethylene was facilitated for higher space velocities, with their selectivities being progressively increased to 10.6 and 20.6%, respectively, with WGHSV increased up to 150,000 mL g^{-1} h^{-1}. On the other hand, carbon monoxide selectivity was monotonically reduced from 15.8 to 1.4% in the entire range of WGHSV used. This implies that the formation of CO through reactions (2), (3) and/or (4) was suppressed as WGHSV increased. The same trends of product selectivities with respect to space velocity were observed at 700 °C, with the values of $S_{C_3H_6}$ (37.3–51.9%) being generally lower and the values of S_{CH_4} (12.0–17.8%) and $S_{C_2H_4}$ (19.9–35.4%) being generally higher compared to those measured at 600 °C (Figure 8b). It is of interest to note that the ratio of propylene to ethylene selectivity goes through a maximum for WGHSV = 6000 mL g^{-1} h^{-1} at both 600 and 700 °C (Figure S4), providing evidence that the C–H bond breaking prevailed over that of C–C breaking for low space velocities, while the opposite occurred as the WGHSV increased from 6000 to 150,000 mL g^{-1} h^{-1}.

Results in Figures 7 and 8 are in excellent agreement with those reported by Michorczyk et al. [22] who found that $Y_{C_3H_6}$ at 600 °C increased with increasing contact time (increasing W/F ratio) using a molar ratio of CO_2:C_3H_8 =7:1 over CrO_x/SiO_2 catalyst, while $S_{C_3H_6}$ remained practically constant and slightly decreased for W/F values higher than 40 g h mol^{-1}. A similar increase in both $X_{C_3H_8}$ and $Y_{C_3H_6}$ at 550 °C with increasing W/F ratio in the range of 0–37.5 g h mol^{-1} was observed over 2.5% Cr_2O_3-ZrO_2 catalyst using a stoichiometric ratio of CO_2:C_3H_8 = 1:1 [21]. The same authors observed that $S_{C_3H_6}$ reached a maximum value for W/F = 7.5 g h mol^{-1} and then gradually decreased as contact time increased further, probably due to carbon formation. Moreover, Wang et al. [61] demonstrated that by decreasing the total flow rate (i.e., increasing the residence time),

higher values of $X_{C_3H_8}$ and $Y_{C_3H_6}$ can be achieved over Fe-doped ceria catalysts in the temperature range of 450–600 °C using a molar ratio of CO_2:C_3H_8 = 1. However, $S_{C_3H_6}$ was found to be decreased monotonically as residence time increased due to the consecutive oxidation of paraffin/olefin to carbon oxides (CO_x). The opposite was observed in the results shown in Figure 8, where $S_{C_3H_6}$ took higher values for higher contact times of catalyst interaction with the reaction mixture, which, as discussed above, was due to suppression of side product formation when the WGHSV was lower.

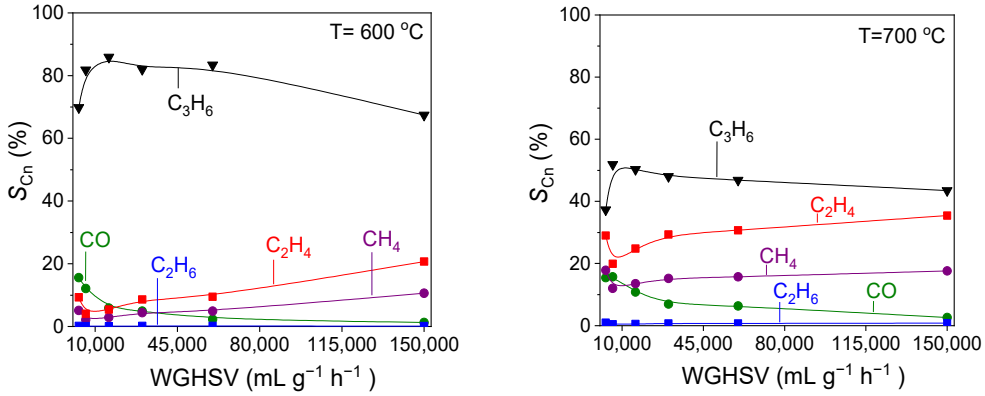

Figure 8. Effect of WGHSV on the selectivities towards reaction products over 10%Ga_2O_3-SiO_2 catalyst at (**a**) 600 and (**b**) 700 °C using a CO_2:C_3H_8 = 5:1.

2.4. Effect of CO_2/C_3H_8 Molar Ratio on Catalytic Performance

Among operating parameters that may affect catalytic performance for the CO_2-ODP reaction is the CO_2:C_3H_8 molar ratio. Thus, its influence was investigated over the 10%Ga_2O_3-SiO_2 catalyst using a WGHSV equal to 6000 h^{-1}. The CO_2:C_3H_8 molar ratio was varied between 1:1 and 10:1 by adjusting CO_2 and C_3H_8 concentrations in the gas stream in the ranges of 5–25% and 2–5%, respectively. It was found that propane conversion did not follow any monotonic trend with increasing CO_2 concentration in the feed (Figure 9a). Specifically, the propane conversion curve was slightly shifted towards higher temperatures with increasing CO_2:C_3H_8 molar ratio from 1:1 to 5:1, while a further increase in this parameter to 10:1 led to propane conversion values similar to those observed for CO_2:C_3H_8 = 5:1 below 700 °C and higher than those observed for CO_2:C_3H_8 = 5:1 above 700 °C. This behavior may be due to the participation of CO_2 in more than one reaction, namely the CO_2-ODP (2), the RWGS (3) and the reverse Boudouard reaction (4), each of which may be affected to a different extent by the CO_2 content in the feed. A more pronounced trend was observed for propylene yield at temperatures of practical interest (<700 °C), where $Y_{C_3H_6}$ was gradually decreased by increasing the CO_2:C_3H_8 molar ratio from 10:1 to 1:1 (Figure 9b). Although this decrease was not too high (from 18 to 13% at 650 °C), it indicates that propylene production cannot be further improved by using higher CO_2 concentrations in the reaction mixture.

Results for product distribution with temperature obtained for the three CO_2:C_3H_8 molar ratios investigated are presented in Figure S5, where only small differences can be observed by increasing the CO_2 content in the gas stream and seem to depend on the reaction temperature. These differences can be better seen in Figure 10, where the selectivities towards reaction products were plotted as a function of the CO_2:C_3H_8 molar ratio at 600 and 700 °C. A small increase in $S_{C_3H_6}$ from 77 to 82% by increasing the CO_2:C_3H_8 molar ratio from 1:1 to 10:1 was observed at 600 °C, which was accompanied by a decrease in S_{CH_4} and $S_{C_2H_4}$ from 6 to 3% and from 11 to 4.5%, respectively, while S_{CO} and $S_{C_2H_6}$ remained practically unchanged (Figure 10a). On the other hand, $S_{C_3H_6}$ and S_{CO} measured at 700 °C were optimized for CO_2:C_3H_8 = 5:1 at 52 and 16%, respectively, at which S_{CH_4} (12%) and $S_{C_2H_4}$ (20%) were minimized (Figure 10b).

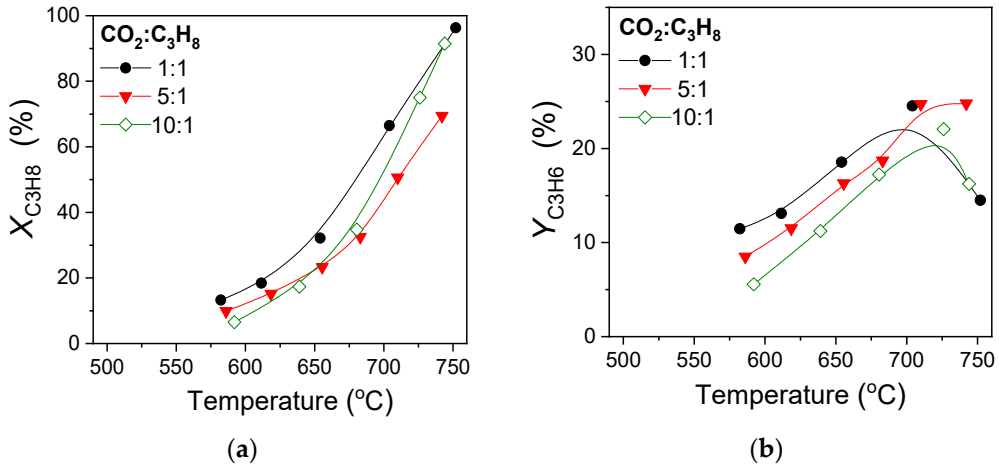

Figure 9. Effect of CO_2:C_3H_8 molar ratio on the (**a**) conversion of C_3H_8 and (**b**) yield of C_3H_6 over 10%Ga_2O_3-SiO_2 catalyst using a WGHSV = 6000 h^{-1}.

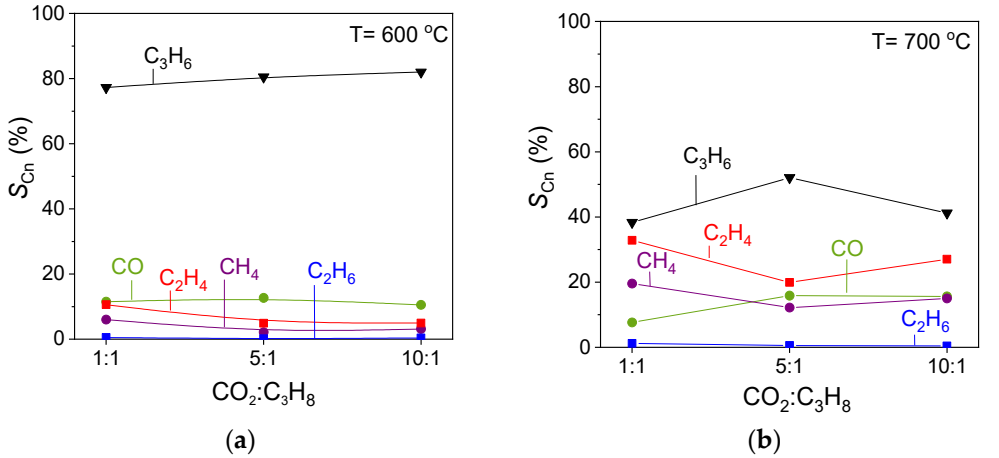

Figure 10. Effect of CO_2:C_3H_8 molar ratio on the selectivities towards reaction products over 10%Ga_2O_3-SiO_2 catalyst at (**a**) 600 and (**b**) 700 °C using a WGHSV = 6000 h^{-1}.

Results reported in the literature regarding the effect of the CO_2:C_3H_8 molar ratio on the catalytic activity for the CO_2-ODP reaction are often contradicting and seem to strongly depend on the catalyst employed. For example, Al-Shafei et al. [62] found that although propane conversion decreased as the CO_2:C_3H_8 molar ratio was raised from 1.4:1 to 12.2:1 over ZrO_2-TiO_2 catalyst, propylene yield was enhanced, accompanied by an increase in the produced propylene/ethylene ratio and an enhancement of the RWGS reaction against the dry propane reforming. According to the authors, these findings indicated that the C–H bond breaking was facilitated compared to that of C–C bond, providing a clear advantage in the process efficiency. An increase in the $S_{C_3H_6}/S_{C_2H_4}$ ratio at both 600 and 700 °C was also observed in the results of the present study by increasing the CO_2:C_3H_8 molar ratio from 1:1 to 5:1, which, however, decreased for CO_2:C_3H_8 = 10:1 (Figure S6). This implies that the rate of C–H bond cleavage against that of C–C bond can be optimized by the appropriate selection of CO_2 and C_3H_8 partial pressures in the gas stream. Moreover, Tian et al. [63] stated that the rate of the RWGS was decreased by decreasing the CO_2:C_3H_8 ratio in the feed from 4:1 to 1:4 over In/HZSM-5 catalyst, which was followed by an enhancement of propane cracking when propane was used in excess. It should be noted, however, that for CO_2:C_3H_8 ratios between 1:1 and 4:1, the variation in product selectivity was not significant, in agreement with the results in Figure S5 and Figure 10. Contrarily, a negative effect of the CO_2 partial pressure in the feed on the $S_{C_3H_6}$ was found over Fe-doped ceria catalyst (accompanied by a slight decrease in propane conversion),

which was attributed to the promotion of the propane dry reforming pathway instead of propane dehydrogenation [61]. A limited negative effect on propane conversion was also found to be induced by increasing the CO_2 concentration in the reaction mixture over 5%Ga_2O_3-SiO_2 catalyst [13]. Moreover, Liu et al. [59] reported that although catalytic activity and stability were significantly improved by the introduction of CO_2 into the feed, propane conversion was slightly decreased by increasing the CO_2:C_3H_8 ratio from 0.5:1 to 3:1, which led researchers to conclude that low concentrations of CO_2 were sufficient for these improvements.

Regarding the results of the present study, since $X_{C_3H_8}$ was not practically affected by the CO_2 content in the gas stream (Figure 9) and the ratio of propylene (desired product) to ethylene (undesired product) selectivity was optimized for a CO_2:C_3H_8 molar ratio of 5:1 (Figure 10 and Figure S6), no further improvement is expected by using either lower or higher CO_2:C_3H_8 molar ratios in the feed stream; therefore, this parameter was not further investigated.

2.5. In Situ DRIFTS Studies for the CO_2-Assisted Oxidative Dehydrogenation of Propane

In situ DRIFTS experiments were carried out under reaction conditions over the least active SiO_2 and the most active Cr_2O_3-SiO_2 catalysts in order to identify the reaction intermediates and correlate them with catalytic activity. In these experiments, the catalyst was exposed to a gas stream consisting of 1%C_3H_8 + 5%CO_2/He at 25 °C, followed by a stepwise increase in temperature up to 500 °C. Results obtained are presented in Figure S7, where it can be seen that the spectrum collected at 25 °C for SiO_2 support (Figure S7a,c, trace a) consisted of (a) one band at 1625 cm^{-1} previously assigned either to bicarbonate species or most possibly to water OH bending [64], since CO_2 can be only barely adsorbed on silica surface in order to give rise to bands in the carbonate region [65,66]; (b) two negative bands at 3735 and 3580 cm^{-1}, attributed to surface OH groups of SiO_2 acting as adsorption sites for CO_2 [65,67]; and (c) six bands in the C–H stretching (ν) region (3000–2850 cm^{-1}) due to asymmetric and symmetric C–H stretching vibrations in methyl ($CH_{3,ad}$) and methylene groups ($CH_{2,ad}$) [26,64,68,69], as well as to gas phase propane [26,68,69] (Table S2). A progressive increase in temperature led to a decrease in the relative intensity of all bands, with that located at 1625 cm^{-1} practically disappearing above 150 °C. A new weak band could be discerned at 3735 cm^{-1} above 400 °C due to hydroxyl surface groups generated by adsorption of steam that may be formed via the RWGS reaction [3,70].

The spectrum obtained at 25 °C from the most active Cr_2O_3-SiO_2 catalyst (Figure S7b,d, trace a) was qualitatively similar to that obtained for bare SiO_2. However, new bands were developed below 1700 cm^{-1} with increasing temperature. Specifically, two bands located at 1559 and 1439 cm^{-1} appeared at 200 °C and 300 °C, respectively. The former was due to bidentate carbonates, and the latter to bicarbonates associated with Cr_2O_3 [26,66,71,72]. Bicarbonate species adsorbed on Cr_2O_3 were also found to contribute to the band detected at 1626 cm^{-1} as early as 25 °C [71]. The relative intensity of the 1559 and 1439 cm^{-1} bands increased with increasing temperature and could be clearly distinguished up to 500 °C (Figure S7b, trace j), indicating that the corresponding species were strongly adsorbed on the catalyst surface. Results imply that the addition of Cr_2O_3 on SiO_2 surface promoted the adsorption and activation of CO_2, which is beneficial for the participation of CO_2 in the propane oxidative dehydrogenation pathway. This is most possibly due to the increased basicity found for Cr_2O_3-SiO_2 catalyst compared to that of bare SiO_2 (Figure 1, Table 2). It is worth noting that a fraction of bidentate carbonates and bicarbonates may be derived by adsorption of CO, which, as discussed above, was among the main reaction products (Figure 4). Interestingly, the band located at 3734 cm^{-1} due to adsorbed H_2O appeared at lower temperature (300 °C, Figure S7b, trace f) for Cr_2O_3-SiO_2 catalyst and was accompanied by a new band at 3582 cm^{-1} that has been reported to arise from H_2O interaction with weak basic OH groups of the metal oxide support [70]. Both bands increased in intensity

with increasing temperature, indicating that H_2O formation/adsorption was favored, most possibly due to the higher activity of the Cr_2O_3 modified catalyst.

The activation and dissociative adsorption of propane on the catalyst surface was confirmed by the detection of bands in the C–H stretching region (3000–2850 cm^{-1}) already at 25 °C for both catalysts investigated. The results imply that although both catalysts were able to activate propane at low temperatures, CO_2 activation was enhanced in the presence of Cr_2O_3, most possibly due to the higher surface basicity induced by its addition on SiO_2 surface. This supports further our suggestion that the number and strength of basic sites on the catalyst surface play a decisive role in propylene production. Moreover, it has been reported that the basic sites may also inhibit the adsorption of the undesired alkenes (produced during alkane oxidative dehydrogenation reactions) on the catalytic active sites, further hindering their deep oxidation to CO, CO_2 or oxygenate species and further benefiting the process [73].

Concerning the reaction mechanism, two general schemes have been proposed for the CO_2-ODP reaction, with the role of CO_2 varying depending on the type of catalyst employed [3,8,55]. According to the first scheme (one-step oxidative route), which dominates over reducible metal oxides like Cr_2O_3, CO_2 participates in the reaction through the Mars–Van Krevelen mechanism. Specifically, hydrogen derived from C_3H_8 dehydrogenation interacts with the lattice oxygen of metal oxides, producing water and oxygen vacancies, while oxygen vacancies are then replenished by oxygen generated via the CO_2 dissociation to complete the redox cycle. According to the second scheme (two-step oxidative route), which is favored over irreducible metal oxides like Ga_2O_3, hydrogen produced from the C_3H_8 dehydrogenation is removed by CO_2 via the RWGS reaction, thus shifting the thermodynamic equilibrium towards propylene production.

Regardless of which mechanism is predominant, CO_2 and propane activation/adsorption on the catalytic basic and acidic sites, respectively, appear to be the key steps for the initiation of the ODP reaction and the efficient production of propylene. Although results of the present study are not able to fully elucidate the mechanistic pathway of the reaction, they provide clear evidence that moderately basic and acidic sites must coexist on the catalyst surface in order to achieve high propylene yields and eliminate the undesired reactions that can lead to the formation of undesirable hydrocarbons (CH_4, C_2H_x), coke and/or deep oxidation products.

3. Materials and Methods

3.1. Catalyst Synthesis and Characterization

M_xO_y-SiO_2 (M: Ca, Sn, Cr, Ga) catalysts were prepared by impregnation of commercial SiO_2 (Alfa Aesar, Kandel, Germany) powder in an aqueous solution of the corresponding metal oxide precursor salt ($Cr(NO_3)_3$ (Thermo Scientific, Waltham, MA, USA), $Ga(NO_3)_3{\cdot}6H_2O$ (Sigma Aldrich, Darmstadt, Germany), $Ca(NO_3)_2{\cdot}4H_2O$ (Thermo Scientific, Waltham, MA, USA), and $SnCl_2{\cdot}2H_2O$ (Sigma Aldrich, Darmstadt, Germany)). Impregnation was followed by drying of the samples at 110 °C overnight and calcination in air at 600 °C for 3 h. The nominal content of M_xO_y was in all cases equal to 10 wt.%. The 10%Ga_2O_3-SiO_2 catalyst was also synthesized in the form of pellets by adding SiO_2 pellets (Thermo Scientific, Waltham, MA, USA) in an aqueous solution of $Ga(NO_3)_3{\cdot}6H_2O$ contained in a BUCHI beaker. The beaker was adjusted in a rotary evaporator, operated at 70 °C under vacuum, that was used to remove water. The pellets were then dried overnight at 110 °C and calcined in air at 600 °C for 3 h.

Catalysts were characterized with respect to their specific surface area and pore volume, phase composition and crystallite size as well as surface basicity and acidity by means of nitrogen physisorption at −196 °C (B.E.T. technique), X-ray diffraction (XRD), temperature-programmed desorption of CO_2 (CO_2-TPD) and pyridine adsorption/desorption experiments, respectively. A Quantachrome gas sorption system (Quantachrome instruments, Boynton Beach, FL 33426, USA) was used to determine the SSA and the total pore volume of composite metal oxides following drying of the samples at 110 °C

for 2 h and by conducting nitrogen adsorption measurements at −196 °C according to the procedure described in detail elsewhere [52]. The Brunauer–Emmett–Teller (BET) method was used to estimate the SSA, while the Barrett–Joyner–Halenda (BJH) method was applied for the total pore volume estimation. A Bruker D8 Advance instrument (Billerica, MA, USA) equipped with a Cu-Kα radiation (λ = 0.15496 nm) source and operated at 40 kV and 40 mA was used for the conduction of XRD analyses. The samples were scanned over a range of 2θ = 20–80° at a scanning rate of 0.05 °/s.

An Omnistar (Pfeiffer Vacuum, Asslar, Germany) mass spectrometer (MS) directly connected to the outlet of a fixed bed reactor was used to determine the surface basicity of the modified silica-based catalysts by employing the temperature-programmed desorption of CO_2 (CO_2-TPD) technique. In these experiments, 0.15 g of catalyst was introduced to the reactor and heated at 450 °C in He flow (40 cm^3 min^{-1}) for 15 min to remove any adsorbed impurities from the catalyst surface, followed by a decrease in temperature at 25 °C. A gaseous mixture consisting of 5% CO_2/He was then introduced to the reactor by controlling the flow by means of mass flow controllers (Brooks Instrument, Hatfield, PA, USA). After 30 min of adsorption, the physisorbed CO_2 was removed by flowing He for 30 min. The TPD was then initiated using a rate of linear temperature rise equal to 10 °C/min until complete desorption of CO_2 from the catalyst surface. During the CO_2-TPD, the transient-MS signals at m/z = 18 (H_2O), 28 (CO) and 44 (CO_2) were continuously recorded.

The surface acidity of catalysts was investigated by pyridine adsorption/desorption experiments employing ex situ DRIFTS. Experiments were conducted in an FTIR (Nicolet iS20, Thermo Fischer Scientific, Waltham, MA, USA) spectrometer equipped with an MCT detector, a KBr beam splitter and a diffuse reflectance cell (Specac, Orpington, UK). In these experiments, 60 mg of catalyst powder was dried overnight at 110 °C, followed by cooling at room temperature. The dried catalyst was then suspended in 5%Pyridine/H_2O solution (Sigma Aldrich, Darmstadt, Germany) for 2 h at room temperature until saturation, followed by filtration and drying at 60 °C for 1 h in order to remove water and weakly adsorbed pyridine. Finally, the sample was placed in the DRIFT cell, and the spectrum was recorded by collecting 64 scans with a resolution of 4 cm^{-1}. A gradual rise in temperature was then applied up to 450 °C in He, during which spectra were collected at selected temperatures after the catalyst had been held at each temperature for 3 min. All spectra were normalized by subtracting the background spectra obtained in He flow at the corresponding temperature.

3.2. Catalytic Performance Tests

Catalytic performance tests were carried out in the temperature range of 500–750 °C under ambient pressure using an apparatus that has been described in detail in our previous study [26]. The quartz reactor was loaded with 0.5 g of catalyst (particle diameter: 0.15 < d_p < 0.25 mm) and placed in an electric furnace, where the catalyst was treated in He at 450 °C for 1 h. Catalyst pretreatment was followed by heating at 500 °C under He, and subsequent switch of the flow to the feed stream consisted of 5% C_3H_8 + 25% CO_2 (He balance). In these experiments, the WGHSV was typically equal to 6000 mL g^{-1} h^{-1}. The reactor effluent was analyzed after 30 min of catalyst on stream using a gas chromatograph (Shimadzu 2014, Kyoto, Japan) equipped with two packed columns (Carboxen, Porapak-Q) and two detectors (TCD and FID). Similar measurements were obtained at selected temperatures following an increase in temperature up to 750 °C.

The equations used for the estimation of C_3H_8 conversion ($X_{C_3H_8}$), reaction rate ($r_{C_3H_8}$ in mol s^{-1} $g_{cat}{}^{-1}$), C_3H_6 yield ($Y_{C_3H_6}$) and selectivity towards reaction products (S_{C_n}) were as follows:

$$X_{C_3H_8} = \frac{[C_3H_8]_{in} \cdot F_{in} - [C_3H_8]_{out} \cdot F_{out}}{[C_3H_8]_{in} \cdot F_{in}} \times 100 \quad (5)$$

$$r_{C_3H_8} = \frac{[C_3H_8]_{in} \cdot F_{in} - [C_3H_8]_{out} \cdot F_{out}}{W} \quad (6)$$

$$Y_{C_3H_6} = (X_{C_3H_8} \cdot S_{C_3H_6})/100 \quad (7)$$

$$S_{C_n} = \frac{[C_n] \cdot n}{[CO] + [CH_4] + 2 \cdot ([C_2H_4] + [C_2H_6]) + 3 \cdot ([C_3H_6])} \times 100 \quad (8)$$

where F_{in} and F_{out} represent the inlet and outlet molar flow rate, $[C_3H_8]_{in}$ and $[C_3H_8]_{out}$ refer to the concentrations (v/v) of C_3H_8 in the inlet and outlet of the reactor, respectively, W is the catalyst mass, $[CO]$, $[CH_4]$, $[C_2H_4]$, $[C_2H_6]$ and $[C_3H_6]$ are the concentrations (v/v) of the corresponding products, and n is the number of carbon atoms in each molecule.

Separate experiments were also performed to examine the influence of WGHSV on catalytic activity, where both the catalyst mass and the total flow rate were varied so as to achieve WGHSVs varying in the range of 3000–150,000 mL g^{-1} h^{-1}. The effect of the CO_2:C_3H_8 molar ratio on catalytic performance was also investigated by conducting experiments where this parameter was varied from 1:1 to 10:1.

3.3. In Situ DRIFTS Experiments Under CO_2-ODP Reaction Conditions

In situ DRIFTS experiments were carried out under conditions of CO_2-assisted oxidative dehydrogenation of propane over selected catalysts using the FTIR spectrometer described above. The experimental procedure involved (a) heating of catalyst in He flow at 500 °C, (b) background collection under the same atmosphere as the catalyst was cooled to 25 °C, (c) exposure of catalyst to the reaction mixture consisting of 1%C_3H_8 + 5%CO_2 (in He) followed by spectrum recording after 15 min, and (d) progressively increasing temperature up to 500 °C, during which spectra were collected at selected temperatures after an equilibration period of 15 min.

4. Conclusions

The effect of the type of metal oxide additive in the silica support on the catalytic performance of the CO_2-assisted oxidative dehydrogenation of propane was reported herein, aiming to identify the key physicochemical properties that affect catalytic activity. Both $X_{C_3H_8}$ and $Y_{C_3H_6}$ were notably increased by a factor of 5 and 6.8, respectively, at temperatures of practical interest following the order (bare) SiO_2 < SnO_2-SiO_2~CaO-SiO_2 < Ga_2O_3-SiO_2 < Cr_2O_3-SiO_2, with the superior Cr-containing sample reaching a maximum $Y_{C_3H_6}$ of 28% at 683 °C. The moderate surface basicity of the Ga_2O_3-SiO_2 and Cr_2O_3-SiO_2 catalysts was found to be essential for the selective conversion of propane to propylene and the suppression of side-product generation. This was also the case for surface acidity, which, according to pyridine adsorption/desorption experiments, was found to be moderate for the most active Cr_2O_3-SiO_2. The higher number and strength of acid sites determined for the Ga_2O_3-SiO_2 catalyst may be responsible for its lower activity compared to that of Cr_2O_3-SiO_2. The process efficiency can be enhanced by decreasing the WGHSV, with propylene selectivity reaching an optimum value of 86% at 600 °C for WGHSV = 6000 mL g^{-1} h^{-1}. Although propane conversion was not practically influenced by the CO_2:C_3H_8 molar ratio in the feed stream, propylene formation against side products can be optimized by the appropriate selection of CO_2 and C_3H_8 concentrations. The TOS stability tests conducted over Ga_2O_3-SiO_2 and Cr_2O_3-SiO_2 catalysts showed that the former one exhibited sufficiently stable performance after about 22 h on stream, while the latter presented a decrease in initial propane conversion during the first 5 h, which smoothed out for longer periods of catalyst interaction with the gas stream. However, both catalysts exhibited excellent stability with respect to the selectivity towards propylene production. DRIFTS studies indicated that the adsorption/activation of CO_2 under reaction conditions was enhanced by the addition of Cr_2O_3 on the SiO_2 surface due to the higher surface basicity characterizing this sample.

Supplementary Materials: The following supporting information can be downloaded at: https://www.mdpi.com/article/10.3390/catal14120933/s1, Table S1: Amount of desorbed CO_2 during CO_2-TPD experiments; Table S2: DRIFT band assignments detected over SiO_2 and Cr_2O_3-SiO_2 catalysts following their interaction with a 1%C_3H_8 + 5%CO_2/He mixture in the temperature range of 25–500 °C; Figure S1. X-ray diffraction patterns obtained over SiO_2-based catalysts; Figure S2.

DRIFT spectra obtained from (a) SnO_2-SiO_2 and (b) CaO-SiO_2 catalysts following adsorption of pyridine at 25 °C for 120 min and subsequent stepwise heating at the indicated temperatures under He flow; Figure S3. Effect of WGHSV on the selectivities toward reaction products obtained as a function of reaction temperature over 10%Ga_2O_3-SiO_2 catalyst; Figure S4. Effect of WGHSV on the ratio of propylene selectivity to ethylene selectivity at 600 and 700 °C; Figure S5. Effect of CO_2:C_3H_8 molar ratio on the selectivities toward reaction products obtained as a function of reaction temperature over 10%Ga_2O_3-SiO_2 catalyst; Figure S6. Effect of CO_2:C_3H_8 molar ratio on the ratio of propylene/ethylene selectivities at 600 and 700 °C; Figure S7. DRIFT spectra obtained over (a) SiO_2 and (b) 10%Cr_2O_3-SiO_2 catalysts following interaction with 1% C_3H_8 + 5% CO_2 (in He) in the temperature range of 25–500 °C. The corresponding DRIFT spectra obtained in the 3100–2750 cm^{-1} region are presented in (c) and (d).

Author Contributions: Conceptualization, P.P.; methodology, P.P.; investigation, A.F., G.B. and A.K.; data curation, A.F., G.B., A.K. and P.P.; writing—original draft preparation, A.K. and P.P.; writing—review and editing, A.K. and P.P.; visualization, P.P.; supervision, P.P.; project administration, P.P.; funding acquisition, P.P. All authors have read and agreed to the published version of the manuscript.

Funding: The research project was supported by the Hellenic Foundation for Research and Innovation (H.F.R.I.) under the "2nd Call for H.F.R.I. Research Projects to support Faculty Members & Researchers" (Project Number: 3367).

Data Availability Statement: The original contributions presented in this study are included in the article/Supplementary Materials. Further inquiries can be directed to the corresponding authors.

Conflicts of Interest: The authors declare no conflicts of interest. The funders had no role in the design of the study; in the collection, analyses, or interpretation of data; in the writing of the manuscript; or in the decision to publish the results.

References

1. Wang, Z.-Y.; He, Z.-H.; Li, L.-Y.; Yang, S.-Y.; He, M.-X.; Sun, Y.-C.; Wang, K.; Chen, J.-G.; Liu, Z.-T. Research Progress of CO_2 Oxidative Dehydrogenation of Propane to Propylene over Cr-Free Metal Catalysts. *Rare Met.* **2022**, *41*, 2129–2152. [CrossRef] [PubMed]
2. Tedeeva, M.A.; Kustov, A.L.; Pribytkov, P.V.; Kapustin, G.I.; Leonov, A.V.; Tkachenko, O.P.; Tursunov, O.B.; Evdokimenko, N.D.; Kustov, L.M. Dehydrogenation of Propane in the Presence of CO_2 on GaO_x/SiO_2 Catalyst: Influence of the Texture Characteristics of the Support. *Fuel* **2022**, *313*, 122698. [CrossRef]
3. Han, X.; Yang, Y.; Chen, R.; Zhou, J.; Yang, X.; Wang, X.; Ji, H. One-Dimensional Ga_2O_3-Al_2O_3 Nanofibers with Unsaturated Coordination Ga: Catalytic Dehydrogenation of Propane under CO_2 Atmosphere with Excellent Stability. *J. Colloid. Interface Sci.* **2024**, *666*, 76–87. [CrossRef] [PubMed]
4. Sandupatla, A.S.; Ray, K.; Thaosen, P.; Sivananda, C.; Deo, G. Oxidative Dehydrogenation of Propane over Alumina Supported Vanadia Catalyst—Effect of Carbon Dioxide and Secondary Surface Metal Oxide Additive. *Catal. Today* **2020**, *354*, 176–182. [CrossRef]
5. Gambo, Y.; Adamu, S.; Lucky, R.A.; Ba-Shammakh, M.S.; Hossain, M.M. Decoupling Reaction Network and Designing Robust VO_x/Al_2O_3 Catalyst with Suitable Site Diversity for Promoting CO_2-Mediated Oxidative Dehydrogenation of Propane. *Chem. Eng. J.* **2024**, *479*, 147458. [CrossRef]
6. Lin, Z.; Zuo, H.; Ma, R.; An, H.; Zhao, P.; Liang, K.; Wang, M.; Lu, F.; Zou, G. The Evolution of Surface Species by Steam Pre-Treatment on CrO_x/Al_2O_3 Catalysts for Propane Dehydrogenation. *Mol. Catal.* **2023**, *539*, 113018. [CrossRef]
7. Rogg, S.; Hess, C. CO_2 as a Soft Oxidant for Propane Oxidative Dehydrogenation: A Mechanistic Study Using Operando UV Raman Spectroscopy. *J. CO_2 Util.* **2021**, *50*, 101604. [CrossRef]
8. Chung, I.; Kim, J.; An, J.; Lee, D.; Park, J.; Oh, H.; Yun, Y. Kinetic Modeling of the Oxidative Dehydrogenation of Propane with CO_2 over a CrO_x/SiO_2 Catalyst and Assessment of CO_2 Utilization. *Chem. Eng. J.* **2024**, *494*, 153178. [CrossRef]
9. Mashkin, M.; Tedeeva, M.; Fedorova, A.; Vasiliev, A.; Egorov, A.; Pribytkov, P.; Kalmykov, K.; Kapustin, G.; Morozov, I.; Kustov, L.; et al. CrO_x/SiO_2 Mesoporous Catalysts Prepared Using Beta-Cyclodextrin as a Template and Their Catalytic Properties in Propane Oxidative Dehydrogenation in the Presence of Carbon Dioxide. *Microporous Mesoporous Mater.* **2022**, *338*, 111967. [CrossRef]
10. Michorczyk, P.; Ogonowski, J.; Zeńczak, K. Activity of Chromium Oxide Deposited on Different Silica Supports in the Dehydrogenation of Propane with CO_2—A Comparative Study. *J. Mol. Catal. A Chem.* **2011**, *349*, 1–12. [CrossRef]
11. Gashoul Daresibi, F.; Khodadadi, A.A.; Mortazavi, Y. Atomic Layer Deposition of Ga_2O_3 on γ-Al_2O_3 Catalysts with Higher Interactions and Improved Activity and Propylene Selectivity in CO_2-Assisted Oxidative Dehydrogenation of Propane. *Appl. Catal. A Gen.* **2023**, *655*, 119117. [CrossRef]

12. Gashoul Daresibi, F.; Khodadadi, A.A.; Mortazavi, Y.; Huotari, S.; Ritala, M. Highly Dispersed Atomic Layer Deposited CrO_x on SiO_2 Catalyst with Enhanced Yield of Propylene for CO_2–Mediated Oxidative Dehydrogenation of Propane. *Mol. Catal.* **2022**, *526*, 112396. [CrossRef]
13. Xu, B.; Zheng, B.; Hua, W.; Yue, Y.; Gao, Z. Support Effect in Dehydrogenation of Propane in the Presence of CO_2 over Supported Gallium Oxide Catalysts. *J. Catal.* **2006**, *239*, 470–477. [CrossRef]
14. Chen, M.; Xu, J.; Su, F.; Liu, Y.; Cao, Y.; He, H.; Fan, K. Dehydrogenation of Propane over Spinel-Type Gallia–Alumina Solid Solution Catalysts. *J. Catal.* **2008**, *256*, 293–300. [CrossRef]
15. Chen, M.; Xu, J.; Liu, Y.-M.; Cao, Y.; He, H.-Y.; Zhuang, J.-H.; Fan, K.-N. Enhanced Activity of Spinel-Type Ga_2O_3–Al_2O_3 Mixed Oxide for the Dehydrogenation of Propane in the Presence of CO_2. *Catal. Lett.* **2008**, *124*, 369–375. [CrossRef]
16. Kocoń, M.; Michorczyk, P.; Ogonowski, J. Effect of Supports on Catalytic Activity of Chromium Oxide-Based Catalysts in the Dehydrogenation of Propane with CO_2. *Catal. Lett.* **2005**, *101*, 53–57. [CrossRef]
17. Chen, M.; Wu, J.-L.; Liu, Y.-M.; Cao, Y.; Guo, L.; He, H.-Y.; Fan, K.-N. Study in Support Effect of In_2O_3/MO_x (M=Al, Si, Zr) Catalysts for Dehydrogenation of Propane in the Presence of CO_2. *Appl. Catal. A Gen.* **2011**, *407*, 20–28. [CrossRef]
18. Atanga, M.A.; Rezaei, F.; Jawad, A.; Fitch, M.; Rownaghi, A.A. Oxidative Dehydrogenation of Propane to Propylene with Carbon Dioxide. *Appl. Catal. B* **2018**, *220*, 429–445. [CrossRef]
19. de Oliveira, J.F.S.; Volanti, D.P.; Bueno, J.M.C.; Ferreira, A.P. Effect of CO_2 in the Oxidative Dehydrogenation Reaction of Propane over Cr/ZrO_2 Catalysts. *Appl. Catal. A Gen.* **2018**, *558*, 55–66. [CrossRef]
20. Chen, S.; Chang, X.; Sun, G.; Zhang, T.; Xu, Y.; Wang, Y.; Pei, C.; Gong, J. Propane Dehydrogenation: Catalyst Development, New Chemistry, and Emerging Technologies. *Chem. Soc. Rev.* **2021**, *50*, 3315–3354. [CrossRef]
21. Singh, R.; Nayak, S.C.; Singh, R.; Deo, G. O_2 and CO_2 Assisted Oxidative Dehydrogenation of Propane Using ZrO_2 Supported Vanadium and Chromium Oxide Catalysts. *Catal. Today* **2024**, *432*, 114617. [CrossRef]
22. Michorczyk, P.; Ogonowski, J. Role of CO_2 in Dehydrogenation of Propane over CrO_X/SiO_2 Catalyst with Low Cr Content. *React. Kinet. Catal. Lett.* **2007**, *92*, 61–68. [CrossRef]
23. Michorczyk, P.; Kuśtrowski, P.; Chmielarz, L.; Ogonowski, J. Influence of Redox Properties on the Activity of Iron Oxide Catalysts in Dehydrogenation of Propane with CO_2. *React. Kinet. Catal. Lett.* **2004**, *82*, 121–130. [CrossRef]
24. Ren, Y.; Zhang, F.; Hua, W.; Yue, Y.; Gao, Z. ZnO Supported on High Silica HZSM-5 as New Catalysts for Dehydrogenation of Propane to Propene in the Presence of CO_2. *Catal. Today* **2009**, *148*, 316–322. [CrossRef]
25. Zhang, K.; Sun, S.; Huang, K. Combined Carbon Capture and Catalytic Oxidative Dehydrogenation of Propane to Propylene Conversion through a Plug-Flow Dual-Phase Membrane Reactor. *Chem. Eng. J.* **2024**, *481*, 148395. [CrossRef]
26. Florou, A.; Bampos, G.; Natsi, P.D.; Kokka, A.; Panagiotopoulou, P. Propylene Production via Oxidative Dehydrogenation of Propane with Carbon Dioxide over Composite M_xO_y-TiO_2 Catalysts. *Nanomaterials* **2023**, *14*, 86. [CrossRef]
27. Kokka, A.; Ramantani, T.; Yentekakis, I.V.; Panagiotopoulou, P. Catalytic Performance and in Situ DRIFTS Studies of Propane and Simulated LPG Steam Reforming Reactions on Rh Nanoparticles Dispersed on Composite M_xO_y-Al_2O_3 (M: Ti, Y, Zr, La, Ce, Nd, Gd) Supports. *Appl. Catal. B* **2022**, *316*, 121668. [CrossRef]
28. Mazumder, J.; de Lasa, H. Fluidizable Ni/La_2O_3-γ-Al_2O_3 Catalyst for Steam Gasification of a Cellulosic Biomass Surrogate. *Appl. Catal. B* **2014**, *160–161*, 67–79. [CrossRef]
29. Al-Ghamdi, S.A.; de Lasa, H.I. Propylene Production via Propane Oxidative Dehydrogenation over VO_x/γ-Al_2O_3 Catalyst. *Fuel* **2014**, *128*, 120–140. [CrossRef]
30. Jawad, A.; Ahmed, S. Analysis and Process Evaluation of Metal Dopant (Zr, Cr)-Promoted Ga-Modified ZSM-5 for the Oxidative Dehydrogenation of Propane in the Presence and Absence of CO_2. *RSC Adv.* **2023**, *13*, 11081–11095. [CrossRef] [PubMed]
31. Igonina, M.; Tedeeva, M.; Kalmykov, K.; Kapustin, G.; Nissenbaum, V.; Mishin, I.; Pribytkov, P.; Dunaev, S.; Kustov, L.; Kustov, A. Properties of CrO_x/MCM-41 and Its Catalytic Activity in the Reaction of Propane Dehydrogenation in the Presence of CO_2. *Catalysts* **2023**, *13*, 906. [CrossRef]
32. Gao, M.; Jiang, H.; Zhang, M. Influences of Interactive Effect Between ZrO_2 and Nano-SiO_2 on the Formation of 1,3-Butadiene from Ethanol and Acetaldehyde. *Catal. Surv. Asia* **2020**, *24*, 115–122. [CrossRef]
33. Sirikulbodee, P.; Phongaksorn, M.; Sornchamni, T.; Ratana, T.; Tungkamani, S. Effect of Different Iron Phases of Fe/SiO_2 Catalyst in CO_2 Hydrogenation under Mild Conditions. *Catalysts* **2022**, *12*, 698. [CrossRef]
34. Zhang, H.; Li, M.; Xiao, P.; Liu, D.; Zou, C.J. Structure and Catalytic Performance of Mg-SBA-15-Supported Nickel Catalysts for CO_2 Reforming of Methane to Syngas. *Chem. Eng. Technol.* **2013**, *36*, 1701–1707. [CrossRef]
35. Cheng, S.; Metzger, L.E.; Martínez-Monteagudo, S.I. One-Pot Synthesis of Sweetening Syrup from Lactose. *Sci. Rep.* **2020**, *10*, 2730. [CrossRef] [PubMed]
36. Al-Muhtaseb, A.H.; Jamil, F.; Osman, A.I.; Tay Zar Myint, M.; Htet Kyaw, H.; Al-Hajri, R.; Hussain, M.; Ahmad, M.N.; Naushad, M. State-of-the-Art Novel Catalyst Synthesised from Waste Glassware and Eggshells for Cleaner Fuel Production. *Fuel* **2022**, *330*, 125526. [CrossRef]
37. Marliza, T.S.; Yarmo, M.A.; Hakim, A.; Tahari, M.N.A.; Hisham, M.W.M.; Taufiq-Yap, Y.H. CO_2 Capture on NiO Supported Imidazolium-Based Ionic Liquid. *AIP Conf. Proc.* **2017**, *1838*, 020008.
38. Zăvoianu, R.; Pavel, O.; Cruceanu, A.; Preda, C.; Niţu, C.; Angelescu, E. Characterization of Silica Supported $NiMoO_4$ Doped with Ce, Cr and Zr Using Thermodesorption Techniques. *Prog. Catal.* **2003**, *12*, 83–92.

39. Constantinou, D.A.; Fierro, J.L.G.; Efstathiou, A.M. The Phenol Steam Reforming Reaction towards H_2 Production on Natural Calcite. *Appl. Catal. B* **2009**, *90*, 347–359. [CrossRef]
40. Burri, D.R.; Choi, K.-M.; Han, D.-S.; Sujandi; Jiang, N.; Burri, A.; Park, S.-E. Oxidative Dehydrogenation of Ethylbenzene to Styrene with CO_2 over SnO_2–ZrO_2 Mixed Oxide Nanocomposite Catalysts. *Catal. Today* **2008**, *131*, 173–178. [CrossRef]
41. Castro-Fernández, P.; Mance, D.; Liu, C.; Moroz, I.B.; Abdala, P.M.; Pidko, E.A.; Copéret, C.; Fedorov, A.; Müller, C.R. Propane Dehydrogenation on Ga_2O_3-Based Catalysts: Contrasting Performance with Coordination Environment and Acidity of Surface Sites. *ACS Catal.* **2021**, *11*, 907–924. [CrossRef]
42. Connell, G.; Dumesic, J.A. The Generation of Brønsted and Lewis Acid Sites on the Surface of Silica by Addition of Dopant Cations. *J. Catal.* **1987**, *105*, 285–298. [CrossRef]
43. Al-Dughaither, A.S.; de Lasa, H. HZSM-5 Zeolites with Different SiO_2/Al_2O_3 Ratios. Characterization and NH_3 Desorption Kinetics. *Ind. Eng. Chem. Res.* **2014**, *53*, 15303–15316. [CrossRef]
44. Otero Areán, C.; Rodríguez Delgado, M.; Montouillout, V.; Lavalley, J.C.; Fernandez, C.; Cuart Pascual, J.J.; Parra, J.B. NMR and FTIR Spectroscopic Studies on the Acidity of Gallia–Silica Prepared by a Sol–Gel Route. *Microporous Mesoporous Mater.* **2004**, *67*, 259–264. [CrossRef]
45. Torres, C.; Rostom, S.; de Lasa, H. An Eco-Friendly Fluidizable FexOy/CaO-γ-Al_2O_3 Catalyst for Tar Cracking during Biomass Gasification. *Catalysts* **2020**, *10*, 806. [CrossRef]
46. Kung, M.C.; Kung, H.H. IR Studies of NH_3, Pyridine, CO, and NO Adsorbed on Transition Metal Oxides. *Catal. Rev.* **1985**, *27*, 425–460. [CrossRef]
47. Salas, P.; Hernández, J.G.; López-Salinas, E.; Schifter, I.; Llanos, M.E.; Navarrete, J.; Morales, J. Sulfated SnO_2-SiO_2 Superacid Catalysts by Sol-Gel Method. *J. Porous Mater.* **1996**, *3*, 241–245. [CrossRef]
48. Wang, S.; Ma, X.; Gong, J.; Yang, X.; Guo, H.; Xu, G. Transesterification of Dimethyl Oxalate with Phenol under SnO_2/SiO_2 Catalysts. *Ind. Eng. Chem. Res.* **2004**, *43*, 4027–4030. [CrossRef]
49. Lueangchaichaweng, W.; Brooks, N.R.; Fiorilli, S.; Gobechiya, E.; Lin, K.; Li, L.; Parres-Esclapez, S.; Javon, E.; Bals, S.; Van Tendeloo, G.; et al. Gallium Oxide Nanorods: Novel, Template-Free Synthesis and High Catalytic Activity in Epoxidation Reactions. *Angew. Chem. Int. Ed.* **2014**, *53*, 1585–1589. [CrossRef] [PubMed]
50. Chen, F.; Shen, K.; Yang, Y.; Huang, H.; Li, Y. MOF-Assisted Synthesis of Highly Mesoporous Cr_2O_3/SiO_2 Nanohybrids for Efficient Lewis-Acid-Catalyzed Reactions. *ACS Appl. Mater. Interfaces* **2020**, *12*, 48691–48699. [CrossRef] [PubMed]
51. Zhou, S.Z.; Gao, X.Q.; Wu, F.; Li, W.C.; Lu, A.H. Enriching GaH_x Species via Co-Feeding Hydrogen to Boost Efficient Propane Dehydrogenation over Ga_2O_3/Al_2O_3 Catalysts. *Appl. Catal. A Gen.* **2023**, *668*, 119488. [CrossRef]
52. Florou, A.; Bampos, G.; Natsi, P.D.; Kokka, A.; Panagiotopoulou, P. Support Induced Effects on the Activity and Stability of Ga_2O_3 Based Catalysts for the CO_2-Assisted Oxidative Dehydrogenation of Propane. *J. Environ. Chem. Eng.* **2024**, *12*, 114603. [CrossRef]
53. Panagiotopoulou, P.; Kondarides, D.I. A Comparative Study of the Water-Gas Shift Activity of Pt Catalysts Supported on Single (MO_x) and Composite (MO_x/Al_2O_3, MO_x/TiO_2) Metal Oxide Carriers. *Catal. Today* **2007**, *127*, 319–329. [CrossRef]
54. Takehira, K.; Ohishi, Y.; Shishido, T.; Kawabata, T.; Takaki, K.; Zhang, Q.; Wang, Y. Behavior of Active Sites on Cr-MCM-41 Catalysts during the Dehydrogenation of Propane with CO_2. *J. Catal.* **2004**, *224*, 404–416. [CrossRef]
55. Li, K.-X.; Cai, X.; Liu, H.-B.; Liu, X.-Y.; Shan, Y.-L.; Feng, X.; Chen, D. Recent Progress in the Development of Catalysts for Propane Dehydrogenation in the Presence of CO_2. *React. Chem. Eng.* **2024**, *9*, 1292–1312. [CrossRef]
56. Wang, H.-M.; Chen, Y.; Yan, X.; Lang, W.-Z.; Guo, Y.-J. Cr Doped Mesoporous Silica Spheres for Propane Dehydrogenation in the Presence of CO_2: Effect of Cr Adding Time in Sol-Gel Process. *Microporous Mesoporous Mater.* **2019**, *284*, 69–77. [CrossRef]
57. Agafonov, Y.A.; Gaidai, N.A.; Lapidus, A.L. Propane Dehydrogenation on Chromium Oxide and Gallium Oxide Catalysts in the Presence of CO_2. *Kinet. Catal.* **2018**, *59*, 744–753. [CrossRef]
58. Wang, J.; Song, Y.-H.; Liu, Z.-T.; Liu, Z.-W. Active and Selective Nature of Supported CrO_x for the Oxidative Dehydrogenation of Propane with Carbon Dioxide. *Appl. Catal. B* **2021**, *297*, 120400. [CrossRef]
59. Liu, Y.; Zhang, G.; Wang, J.; Zhu, J.; Zhang, X.; Miller, J.T.; Song, C.; Guo, X. Promoting Propane Dehydrogenation with CO_2 over Ga_2O_3/SiO_2 by Eliminating Ga-Hydrides. *Chin. J. Catal.* **2021**, *42*, 2225–2233. [CrossRef]
60. Michorczyk, P.; Ogonowski, J. Dehydrogenation of Propane in the Presence of Carbon Dioxide over Oxide-Based Catalysts. *React. Kinet. Catal. Lett.* **2003**, *78*, 41–47. [CrossRef]
61. Wang, H.; Tsilomelekis, G. Catalytic Performance and Stability of Fe-Doped CeO_2 in Propane Oxidative Dehydrogenation Using Carbon Dioxide as an Oxidant. *Catal. Sci. Technol.* **2020**, *10*, 4362–4372. [CrossRef]
62. Al-Shafei, E.N.; Brown, D.R.; Katikaneni, S.P.; Al-Badairy, H.; Muraza, O. CO_2-Assisted Propane Dehydrogenation over of Zirconia-Titania Catalysts: Effect of the Carbon Dioxide to Propane Ratios on Olefin Yields. *J. Environ. Chem. Eng.* **2021**, *9*, 104989. [CrossRef]
63. Tian, H.; Liao, J.; Zha, F.; Guo, X.; Tang, X.; Chang, Y.; Ma, X. Catalytic Performance of In/HZSM-5 for Coupling Propane with CO_2 to Propylene. *ChemistrySelect* **2020**, *5*, 3626–3637. [CrossRef]
64. Rafigh, S.M.; Heydarinasab, A. Mesoporous Chitosan–SiO_2 Nanoparticles: Synthesis, Characterization, and CO_2 Adsorption Capacity. *ACS Sustain. Chem. Eng.* **2017**, *5*, 10379–10386. [CrossRef]
65. Bal, R.; Tope, B.B.; Das, T.K.; Hegde, S.G.; Sivasanker, S. Alkali-Loaded Silica, a Solid Base: Investigation by FTIR Spectroscopy of Adsorbed CO_2 and Its Catalytic Activity. *J. Catal.* **2001**, *204*, 358–363. [CrossRef]

66. Pan, Y.; Kuai, P.; Liu, Y.; Ge, Q.; Liu, C. Promotion Effects of Ga_2O_3 on CO_2 Adsorption and Conversion over a SiO_2-Supported Ni Catalyst. *Energy Environ. Sci.* **2010**, *3*, 1322. [CrossRef]
67. Ueno, A.; Bennett, C.O. Infrared Study of CO_2 Adsorption on SiO_2. *J. Catal.* **1978**, *54*, 31–41. [CrossRef]
68. Tóth, A.; Halasi, G.; Bánsági, T.; Solymosi, F. Reactions of Propane with CO_2 over Au Catalysts. *J. Catal.* **2016**, *337*, 57–64. [CrossRef]
69. SolymosiI, F.; Tolmacsov, P.; Zakar, T. Dry Reforming of Propane over Supported Re Catalyst. *J. Catal.* **2005**, *233*, 51–59. [CrossRef]
70. Boudjemaa, A.; Daniel, C.; Mirodatos, C.; Trari, M.; Auroux, A.; Bouarab, R. In Situ DRIFTS Studies of High-Temperature Water-Gas Shift Reaction on Chromium-Free Iron Oxide Catalysts. *Comptes Rendus. Chim.* **2011**, *14*, 534–538. [CrossRef]
71. Zecchina, A.; Coluccia, S.; Guglielminotti, E.; Ghiotti, G. Infrared Study of Surface Properties of .Alpha.-Chromia. III. Adsorption of Carbon Dioxide. *J. Phys. Chem.* **1971**, *75*, 2790–2798. [CrossRef]
72. Bensalem, A.; Weckhuysen, B.M.; Schoonheydt, R.A. Nature of Adsorbed Species during the Reduction of CrO_3/SiO_2 with CO In SituFTIR Spectroscopic Study. *J. Chem. Soc. Faraday Trans.* **1997**, *93*, 4065–4069. [CrossRef]
73. Savova, B.; Filkova, D.; Crişan, D.; Crişan, M.; Răileanu, M.; Drăgan, N.; Galtayries, A.; Védrine, J.C. Neodymium Doped Alkaline-Earth Oxide Catalysts for Propane Oxidative Dehydrogenation. Part I. Catalyst Characterisation. *Appl. Catal. A Gen.* **2009**, *359*, 47–54. [CrossRef]